#### **ORIGINAL PAPER**



# A mathematical model of maternal vascular growth and remodeling and changes in maternal hemodynamics in uncomplicated pregnancy

Rudolph L. Gleason Jr<sup>1,2,3</sup> • Farbod Sedaghati<sup>1,3</sup>

Received: 7 May 2021 / Accepted: 26 December 2021 © The Author(s), under exclusive licence to Springer-Verlag GmbH Germany, part of Springer Nature 2022

#### Abstract

The maternal vasculature undergoes tremendous growth and remodeling (G&R) that enables a > 15-fold increase in blood flow through the uterine vasculature from conception to term. Hemodynamic metrics (e.g., uterine artery pulsatility index, UA-PI) are useful for the prognosis of pregnancy complications; however, improved characterization of the maternal hemodynamics is necessary to improve prognosis. The goal of this paper is to develop a mathematical framework to characterize maternal vascular G&R and hemodynamics in uncomplicated human pregnancies. A validated 1D model of the human vascular tree from the literature was adapted and inlet blood flow waveforms at the ascending aorta at 4 week increments from 0 to 40 weeks of gestation were prescribed. Peripheral resistances of each terminal vessel were adjusted to achieve target flow rates and mean arterial pressure at each gestational age. Vessel growth was governed by wall shear stress (and axial lengthening in uterine vessels), and changes in vessel distensibility were related to vessel growth. Uterine artery velocity waveforms generated from this model closely resembled ultrasound results from the literature. The literature UA-PI values changed significantly across gestation, increasing in the first month of gestation, then dramatically decreasing from 4 to 20 weeks. Our results captured well the time-course of vessel geometry, material properties, and UA-PI. This 1D fluid-G&R model captured the salient hemodynamic features across a broad range of clinical reports and across gestation for uncomplicated human pregnancy. While results capture available data well, this study highlights significant gaps in available data required to better understand vascular remodeling in pregnancy.

tion to term.

Keywords Biomechanics · Uterine artery · Pulsatility index · Preeclampsia · Pulse wave model

### 1 I. Introduction

During pregnancy, the uterine vasculature undergoes unprecedented levels of growth and remodeling (G&R) compared to other vascular beds in adults, characterized by a > twofold increase in vascular caliber, likely coupled with a dramatic increases in vessel length, as the uterus expands > fivefold in diameter and in length due to the growing fetus inside

metrium of the uterus (Fig. 1); this initiating step promotes the transformation of the high-resistance, vasoreactive spiral arteries into low-resistance passive conduits and may promote the formation and remodeling of arteriovenous (AV) shunts (Osol and Moore 1994; James et al. 2017). This local reduction in peripheral resistance increases perfusion of the uterine vasculature, which subsequently initiates G&R of the proximal vasculature to further increase perfusion (Burton et al. 2009). This vascular G&R, combined with a 30–50% increase in cardiac output, enables a 5- to 20-fold increase in blood flow through the uterine vasculature from concep-

(Osol and Moore 1994; Osol and Mandala 2009). Following placentation, extravillous trophoblasts invade the myo-

Impairment of vascular G&R during pregnancy can lead to pregnancy complications, including fetal growth restriction (FGR) and preeclampsia and other forms of pregnancy-induced hypertension. Hemodynamic metrics, such as uterine artery pulsatility index (UA-PI), resistivity

Published online: 02 February 2022



<sup>☐</sup> Rudolph L. Gleason Jr rudy.gleason@me.gatech.edu

The George W. Woodruff School of Mechanical Engineering, Georgia Institute of Technology, Atlanta, GA, USA

The Wallace H. Coulter Georgia Tech/Emory Department of Biomedical Engineering, Georgia Institute of Technology, 387 Technology Circle, Room 205, Atlanta, GA 30313, USA

Parker H. Petit Institute for Bioengineering and Bioscience, Georgia Institute of Technology, Atlanta, GA, USA

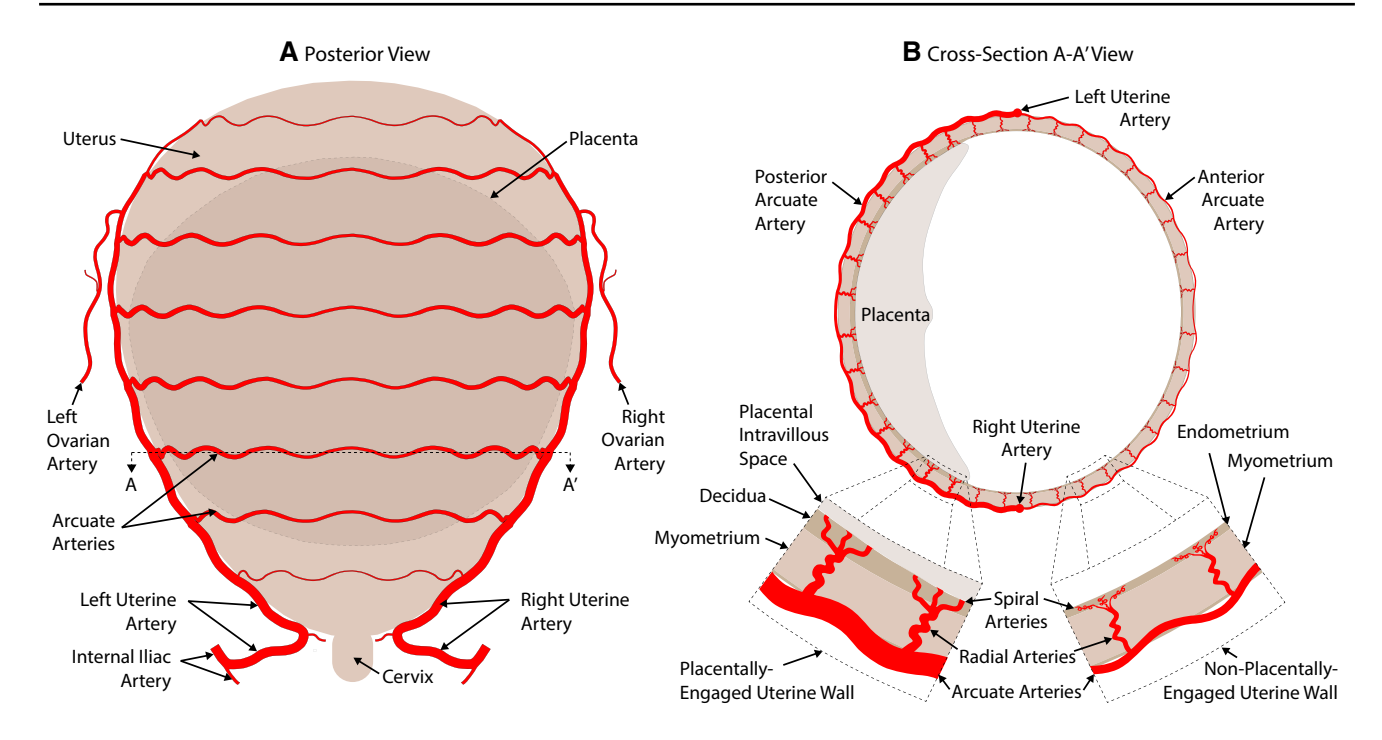


Fig. 1 Illustration of the model uterine vasculature at 36 weeks of gestation. Blood flow to the uterus arises through the right and left uterine artery and the right and left ovarian artery. The uterine arteries arise from the internal iliac arteries. Arcuate arteries branch off the uterine arteries, travel circumferentially along the uterus and

anastomose with the contralateral arcuate arteries. Radial arteries branch from the arcuate arteries and travel radially through the myometrium, bifurcating into the spiral arteries. Placentally engaged spiral arteries supply the intravillous space of the placenta

index, or presence of an early diastolic notch in the uterine artery centerline velocity profile, have shown to be useful as early indicators of risk of pregnancy complications; however, these metrics show only fair prognostic accuracy. Onedimensional computational fluid dynamics models, so-called pulse wave propagation models, provide predictions of the blood pressure, blood flow, and artery diameter waveforms over the cardiac cycle, throughout the vascular tree, and characterize the propagation of blood flow from the heart to peripheral vascular beds (Stergiopulos et al. 1992). The development of a validated pulse wave propagation model of the maternal vasculature (including the uterine vasculature) may provide a useful tool to quantify changes in maternal hemodynamics in healthy pregnancy and to test competing hypotheses regarding impaired vascular G&R that may contribute to the observed difference in maternal hemodynamics with preeclampsia and FGR. While the numbers are few, mathematical models have been reported to capture important features of maternal hemodynamics during pregnancy (Carson et al. 2019; Clark et al. 2018; Corsini et al. 2017; Mo et al. 1988); however, no models to date describe the vascular G&R of the maternal vasculature throughout pregnancy and the consequences of this G&R on the maternal hemodynamics.

The purpose of this paper is to develop a combined 1D hemodynamic model that incorporates vascular G&R for

the human maternal vasculature throughout gestation for uncomplicated pregnancies and validate this model based on available results from the literature. Starting from the vascular network of Reymond et al. (2009), a model uterine vasculature was added and the inlet blood flow waveforms at the aortic sinus at 4 week increments from 0 to 40 weeks of gestation were prescribed. Peripheral resistances of each terminal vessel were iteratively adjusted to achieve target flow rates and mean arterial pressure at each gestational age; these target values were derived from compiled results from the literature. We incorporate shear stress-mediated vascular G&R across the entire maternal vasculature and axial growth of the uterine vasculature in response to the expanding uterus throughout pregnancy. A phenomenological model for changes in vessel distensibility as a function of vessel growth was also employed. Compliance values of each terminal vessel were modestly adjusted to match target values of the systolic blood pressure and UA-PI, derived from compiled results from the literature. Illustrative simulations for high, medium, and low values of cardiac output and uterine flow that span a broad range of published values were performed. Modeling results are compared to a broad set of literature data on changes in maternal vascular geometry and hemodynamics throughout gestation.



#### 2 Methods

# 2.1 One-dimensional modeling theoretical framework

Balance Relations The arterial network was modeled as tapered, elastic tubes in a one-dimensional pulsatile fluid flow framework. Conservation of mass requires that.

$$\frac{\partial A(z,t)}{\partial P(z,t)} \frac{\partial P(z,t)}{\partial t} + \frac{\partial Q(z,t)}{\partial z} = 0. \tag{1}$$

where A(z, t) is the instantaneous arterial lumen cross-sectional area, P(z, t) is the luminal pressure, and Q(z, t) is the volumetric flow rate; z is the direction along the vessel axis, and t is time. The balance of linear momentum requires that

$$\frac{\rho}{A}\frac{\partial Q}{\partial t} + \frac{\partial P}{\partial z} = \frac{f}{A} - \frac{\rho}{A}\frac{\partial}{\partial z}\left(\frac{Q(z,t)^2}{A(z,t)}\right) \tag{2}$$

non-gravid maternal vasculature, we let the reference distensibility  $D_{\text{ref}}$  at  $(P_{\text{ref}} = 100 \text{ mmHg})$  be defined through the empirical relationship,

$$D_{\text{ref}}(\overline{d}, P_{\text{ref}}) = \frac{1}{\rho \left(a_2/\overline{d}^{b_2}\right)^2}$$
 (5)

where  $\overline{d}$  is the reference diameter; we let the parameters  $a_2 = 13.3$  and  $b_2 = 0.30$  (Reymond et al. 2009). The distensibility at any pressure D(P) was calculated as

$$D(P) = \left[ a_1 + \frac{b_1}{1 + \left(\frac{P - P_{\text{max}C}}{P_{\text{width}}}\right)^2} \right] D_{\text{ref}}$$
 (6)

where  $a_1$ =0.4,  $b_1$ =5,  $P_{\text{max}C}$ =2.67 kPa, and  $P_{\text{width}}$ =4.0 kPa. The area compliance  $C_A$  is related to the distensibility as  $C_A$ =DA, which can be integrated to yield an expression for A versus P, as

$$A(P) = A_{\text{ref}} \exp \left\{ a_1 D_{\text{ref}} \left( P - P_{\text{ref}} \right) + b_1 D_{\text{ref}} P_{\text{width}} \left( \tan^{-1} \left( \frac{P - P_{\text{max}C}}{P_{\text{width}}} \right) - \tan^{-1} \left( \frac{P_{\text{ref}} - P_{\text{max}C}}{P_{\text{width}}} \right) \right) \right\}$$
 (7)

where  $\rho$  is the blood density, f is the frictional force per unit length.

Velocity profile approximation. The axial velocity profile,  $u_z(r, z, t)$ , at any instant t and location z is unknown; to proceed, the velocity profile must be approximated so that f can be calculated. No exact solution exists for the velocity profile in a tapered, elastic tube. As done by others (Boom et al. 2018; Boileau et al. 2018), we let

$$u_z(r,z,t) = \overline{u}(z,t) \frac{\zeta + 2}{\zeta} \left[ 1 - \left( \frac{r}{r_i} \right)^{\zeta} \right]$$
 (3)

where  $\overline{u}(z,t) = Q(z,t)/A(z,t)$  is the mean velocity,  $\zeta$  is a constant that governs the shape of the velocity profile, r is the radial coordinate, and  $r_i$  is the lumen radius. By using the Navier–Stokes equations and integrating Eq. (3),

$$f = -2(\zeta + 2)\mu\pi \frac{Q(z,t)}{A(z,t)},\tag{4}$$

where  $\mu$  is the apparent blood viscosity. Given that all vessels are above 250 microns in diameter, the Fahraeus–Lindqvist effects are negligible and a constant value for  $\mu = 4$  mPa-s was prescribed.

Solid Mechanics. Equations (1) and (2) contain three unknowns at each axial location and time, P(x, t), Q(z, t), and A(z, t); a third governing equation arises from solid mechanics that relates applied loads to geometric changes of the artery wall. Following Reymond et al., for the

Boundary conditions at junctions At bifurcations, we impose the continuity of flow and dynamic pressure at each branching point, neglecting minor pressure losses that may occur in the vicinity of the bifurcation. Thus, we let

$$\sum_{i=1}^{N} Q_i(z, t) = 0 \tag{8}$$

$$P_{i}(z,t) + \frac{\rho}{2}\overline{u}_{i}(z,t)^{2} = P_{j}(z,t) + \frac{\rho}{2}\overline{u}_{j}(z,t)^{2} \quad i,j = 1, 2, \dots, N$$
(9)

where i and j denote different vessels of the junction and N represents the total number of branches at the junction.

Terminal boundary conditions. To capture the resistance and compliance of the peripheral vasculature, beyond the terminal artery branches, a three-element Windkessel (WK3) model is applied, which accounts for the proximal resistance ( $R_1$ ), compliance (C), and distal resistance ( $R_2$ ); where the total terminal resistance  $R_T = R_1 + R_2$ . We let  $R_1 = Z_c$ , where  $Z_c$  is the characteristic impedance of the last arterial segment proximal to the terminal WK3, and, following Reymond et al., let  $Z_c = \sqrt{\rho}/(A_{\rm ref}\sqrt{D_{\rm ref}})$ , with values constrained to be within 5–40% of  $R_T$  (Reymond et al. 2009).



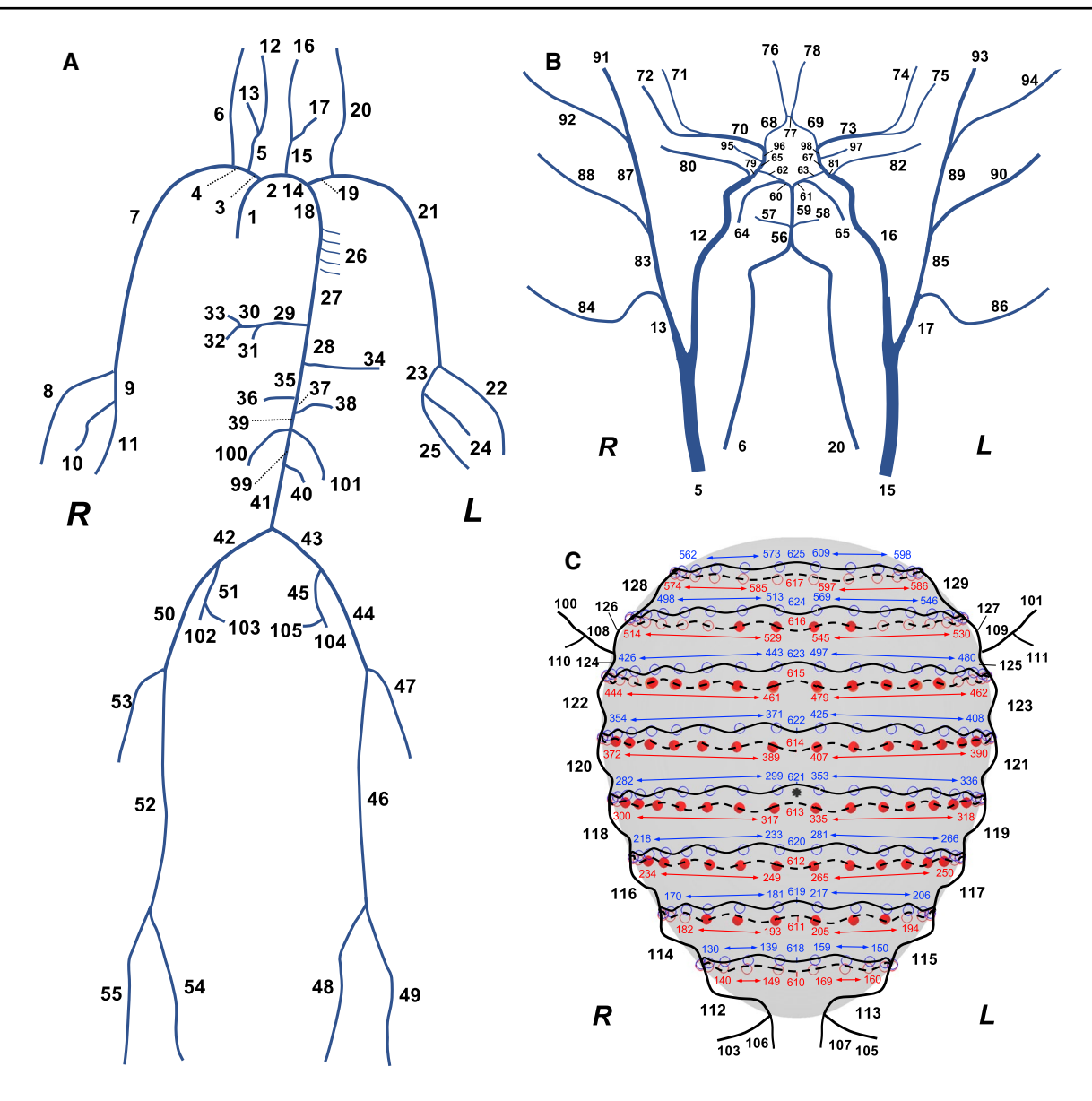


Fig. 2 Schematic representation of the vascular tree. The main systemic vascular network (A) and the cerebral vascular tree (B) were based on the model of Reymond et al., 2009. The model uterine vasculature (C) was developed by overlying tortuous uterine and arcuate arteries (shown as black lines) on geometric models of uteri across gestation. The blue and circles represent the branching points of radial arteries on the anterior and posterior sides of the uterus,

respectively. The closed red circles indicate placentally engaged radial arteries, whereas the open red and blue circles indicate radial arteries that do not communicate to the placenta. The dimensions, properties, and connectivity of each artery segment, for each illustrative simulation and each gestational age are provided in supplemental spreadsheet file entitled "Online Appendix B: Properties Table.xlsx."

# 2.2 Vasculature growth and remodeling throughout gestation

The model vascular network (Fig. 2) was adapted from geometry, distensibility, and peripheral resistances and compliances of the arterial tree presented in Reymond et al. (2009). We adapt this vascular networks in two way. First, we added a model uterine vasculature, consisting of uterine arteries, ovarian arteries, arcuate arteries, radial arteries, and Windkessel elements that represent the spiral arteries,

arterial-venous shunts, capillaries, intervillous space, and the distal venous system. Second, to characterize how the model vasculature and hemodynamics evolve, we prescribed the following across gestation:

- (1) *Inlet boundary conditions*: We prescribe the cardiac output and inlet blood flow waveform at each timepoint in gestation;
- (2) Outlet boundary conditions: Windkessel parameters at terminal sites  $(R_1, R_2, C)$  are prescribed to achieve



target flow rates and mean arterial pressure at each gestational age:

- (3) *Growth*: Vessel radii were adjusted to achieve prescribed target shear stress values in each vessel segment and vessel lengths of the uterine and arcuate arteries both reduced their tortuosity and grew lengthwise to compensate for the growth of the uterus; and
- (4) *Remodeling*: Vessel distensibility of each vessel segment increased as a function of growth.

Based on a review of the literature, we provide our best estimates regarding these throughout gestation that represent well data from multiple data sources, when available, as described in the subsections below.

## 2.2.1 Inlet boundary conditions versus gestation

To establish the inlet blood flow waveform we let

$$Q_{\text{inlet}}(t) = \text{CO} \int_{0}^{t_{c}} q(t) dt$$
 (10)

where CO is the prescribed cardiac output,  $t_c(\sec) = 60/HR$ , HR is the prescribed heartrate in beats per minute (bpm), q(t) describes the shape of the inlet flow waveform, where  $\int_0^{t_c} q(t) dt = 1$ . We digitized the mean of the inlet blood flow waveform presented in Reymond et al. (Fig. 4, panel A, upper curve) to determine q(t) (Reymond et al. 2009). Changes in CO and HR throughout gestation were prescribed based on literature reports and were used to adjust  $t_c$  and  $Q_{inlet}(t)$ .

#### 2.2.2 Outlet boundary conditions versus gestation

We adjusted the terminal resistances  $R_T$  for all the terminal sites such that the MAP matches prescribed values, based on a fit of data from the literature, and that the flow rate through the common iliac, renal, and internal carotid arteries match, as closely as possible, values reported in the literature. To match these values, we altered the limb (i.e., arterial segments 8, 10, 11, 22, 24, 25, 45, 47, 48, 49, 51, 53, 54, and 55), trunk (arterial segments 26, 31, 32, 33, 34, 36, 38, and 40), and cerebral (terminal segments 57, 58, 64, 65, 71, 72, 74, 75, 76, 78, 84, 86, 88, 90, 91, 92, 93, and 94) resistances by the factors,  $f_L$ ,  $f_T$ , and  $f_C$ , respectively. For example, in the non-gravid limbs, the terminal resistances at a given gestational time-point  $R_T=f_LR_T^{\rm Rey}$ , where  $R_T^{\rm Rey}$  are the terminal resistances from the Reymond et al. network. All terminal compliances are prescribed to be inversely related to the terminal resistance for each site; i.e.,  $R_T C_T = a_{RTC}$  where  $a_{\rm RTC}$  was adjusted slightly for each illustrative simulation,

as described below, to achieve the target systolic blood pressure.

For the terminal radial arteries in the uterine vasculature, we iteratively adjusted the  $R_T$  for placental radial arteries, so that the flow through the uterine artery reached target values and the total flow through the non-placental radial arteries remained constant throughout gestation. The compliance of the radial arteries was found as  $R_TC_T = a_{\rm RTC}$ . For the radial arteries of the non-gravid uterine vasculature,  $a_{\rm RTC}$  was adjusted for all radial arteries so that the uterine artery pulsatility index (UA-PI) reached target values. For the gravid uterine vasculature,  $a_{\rm RTC}$  for placentally engaged radial arteries was adjusted so that the UA-PI reached target values;  $a_{\rm RTC}$  for non-placentally engaged radial arteries was set to the value in non-gravid radial arteries.

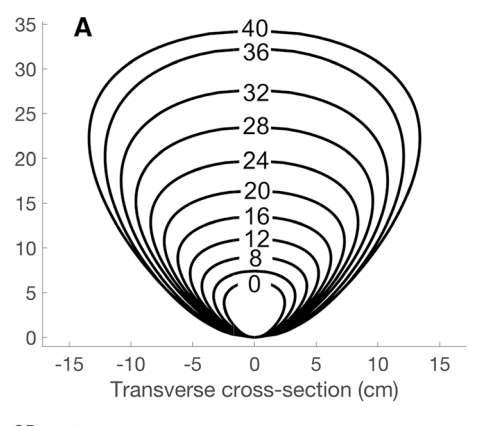
# 2.2.3 Vascular geometry (radii, lengths) versus gestation

Creating model uterine vascular networks across gestation. Uterine arteries arise from the internal iliac artery, travel along the perimetrium and anastomoses the ovarian artery (Figs. 1 and 2). Ovarian arteries arise from the sub-renal abdominal aorta and provide blood flow to the ovaries. The anastomosis between the uterine and ovarian arteries provides an important redundancy for the blood supply to these tissues. Arcuate arteries branch from the uterine arteries, travel circumferentially across the uterus at the level of the myometrium, and often anastomose with the contralateral arcuate arteries, creating another important redundancy in the uterine vasculature (Osol and Moore 1994; Dickey 1997). Radial arteries branch from the arcuate arteries and travel radially through the myometrium and bifurcate into spiral arteries and basal arteries which supply the endometrium. In non-gravid women, spiral arteries terminate to capillaries that collect into venous sinusoids, return to the endometrial veins, myometrial veins, the uterine venous plexus, and internal iliac vein. In gravid women, placentally engaged spiral arteries terminate in the intervillous space, which contain chorionic villi that provide exchange between the fetal and maternal circulation. The intervillous space is drained by endometrial veins, which return flow to the venous circulation.

Model uteri across gestation. To create a model uterine vasculature, we create a model uterus at each gestational age under study, based on literature reports of uterus size (Fig. 3), and overlaid the uterine, arcuate, and radial arteries on the model uteri. We approximate the size of the uterus as an egg shape, using the following equations for the uterus cross section in the coronal plane and sagittal plane

$$\frac{(z-c)^2}{c^2} + \frac{t(z)r_x(z)^2}{a^2} = 1 \quad \text{and} \quad \frac{(z-c)^2}{c^2} + \frac{t(z)r_y(z)^2}{b^2} = 1$$
(11)





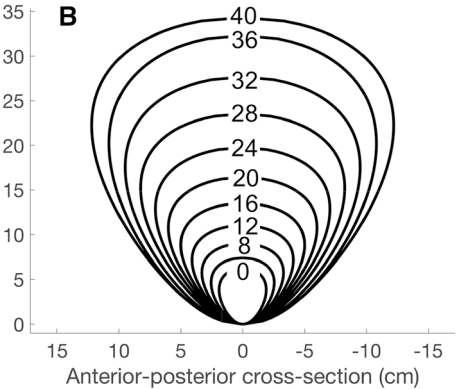


**Fig. 3** Illustration of the coronal **(A)** and sagittal **(B)** cross sections of the model uterus throughout gestation. The numbers along the top edge of the cross sections indicate the gestational age in weeks

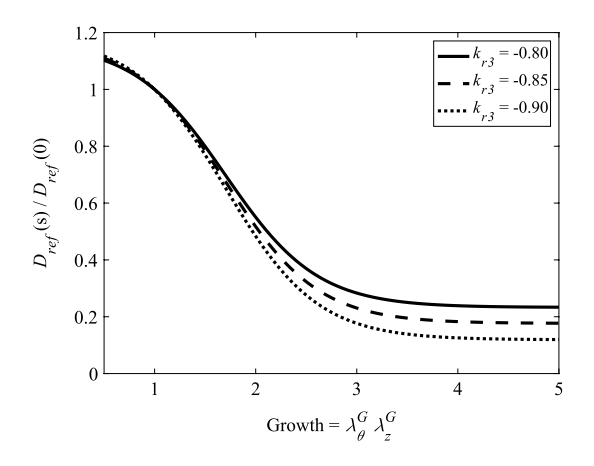


**Fig. 4** Relationship between 'remodeling' (i.e., change in distensibility) and growth with  $k_{r1}$ =2.2 and  $k_{r2}$ =1.7 and  $k_{r3}$ =-0.80, -0.85, and -0.90

where  $r_x(z)$  and  $r_y(z)$  are the distance from the centerline to the uterine wall in the coronal and sagittal planes, z is the axial direction along the uterus midline, a, b, and c are shape parameters related to the mid-uterus diameters in the

transverse, anterior—posterior and midline directions, and t(z), which accounts for the asymmetry in the z direction, is given as t(z) = (1 + kz)/(1 - kz). Equation (11) can be solved for the transverse and anterior—posterior diameters as

$$r_x(z) = \sqrt{\frac{a^2}{t(z)} \left(1 - \frac{(z - c)^2}{c^2}\right)}$$
 and  $r_y(z) = \sqrt{\frac{b^2}{t(z)} \left(1 - \frac{(z - c)^2}{c^2}\right)}$  (12)

The Cartesian components of a surface of the uterine wall are defined by

$$x = r_x \cos(\theta), \quad y = r_y \sin(\theta), \quad z = z$$
 (13)

for z=0 to 2c and  $\theta=0$  to  $2\pi$ . The cross sections of the uterus in the coronal and sagittal planes and geometric parameters for the uterine wall throughout gestation are consistent typical reported values (Jones et al. 1981; Edgar 1910).

Quantifying arcuate artery lengths throughout gestation. Very little data are available on the geometry of arcuate arteries. We used the model uterus to determine the locations and lengths of the arcuate arteries. We overlaid 8 arcuate arteries in each quadrant (anterior right, anterior left, posterior right, and posterior left) of the model uterus (Fig. 2) (Osol and Moore 1994; Dickey 1997; Fernstrom 1955; Chen et al. 2010); each arcuate arises from the right or left uterine artery and terminates in an anastomosis with the contralateral arcuate artery. Arcuate arteries are highly tortuous, in a spiral configuration, in the non-gravid uterus (Chen et al. 2010). The length of each arcuate artery was calculated as  $L_{AA} = \delta_{AA}L_{cl}$ , where  $L_{cl}$  is the arc length of uterus wall over which the arcuate artery travels and  $\delta_{AA}$  is the tortuosity of the arcuate artery. There are no published values of  $\delta_{AA}$ and it is not clear to what degree the arcuate arteries simply 'uncoil' as the uterus expands versus the degree of growth in the axial direction throughout gestation. We calculate  $L_{cl}$ from the model uterus at the level of each prescribed arcuate artery and prescribe values of tortuosity to decrease monotonically from  $\delta_{AA} = 2.25$  in non-gravid uteri to  $\delta_{AA} = 1.05$  at 40 weeks of gestation.

Quantifying uterine artery lengths throughout gestation. Similarly, the model uterus was also used to determine the length of each segment of the uterine artery, between each arcuate artery branch. The uterine arteries was located along the right and left sides of the uterus and the length of each segment was calculated as  $L_{UA} = \delta_{UA} L_{cl}$ , where  $L_{cl}$  is the arc length of uterus wall over which the uterine artery travels and  $\delta_{UA}$  is the tortuosity of the uterine artery. There are no published values of  $\delta_{UA}$ . We calculate  $L_{cl}$  from the model uterus for each uterine artery segment and prescribe values of tortuosity to decrease monotonically from  $\delta_{UA} = 1.80$  in non-gravid uteri to  $\delta_{UA} = 1.05$  at 40 weeks of gestation.



Quantifying radial artery locations. The terminal location of the uterine vasculature was at the mid-myometrial radial artery. Radial arteries terminate with a WK3 that captures the changes in resistance and compliance of the spiral arteries, basal arteries, AV-shunts, and the peripheral venous circulation. Based on histological examination, Brosens and colleagues estimated that there are 120 spiral arteries that terminate in the intervillous space at the 39th week of pregnancy (Brosens and Dixon 1966; Brosens 1964; Brosens et al. 2011, 1967; Robertson 1976). We estimate that the placenta covers ~ 20\% of the uterus; thus, we estimate 600 spiral arteries across the entire uterus. Brosens and Dixon observed that radial arteries typically bifurcate into 2 to 3 spiral arteries; thus, we estimate that there are 240 radial arteries across the entire uterine body. We set the terminal location of the radial artery as 2.5 mm away from the arcuate artery. The location of each branch point of radial arteries, from the arcuate artery, was determined so that the radial arteries were evenly spaced across the entire length of the arcuate arteries.

Adjusting vascular lengths for a representative woman. We consider an average size woman of height 162.5 cm and 62.5 kg and adjust the lengths of all arteries from Reymond et al. by a factor of 162.5/175.5 = 0.9259, where 175.5 cm represents the height of the average man.

Quantifying changes in vascular caliber throughout gestation: Shear stress-mediated growth. It is well established that mechanically mediated vascular growth correlates well with restoration of the wall shear stress and local transmural wall stresses (Kamiya and Togawa 1980; Gleason et al. 2004). The vasculature appears to grow so that the mean wall shear stress  $(\overline{\tau}_w)$  from blood flow is restored to target values  $\overline{\tau}_w^T$ ; for arteries,  $\overline{\tau}_w^T$  generally takes values of 0.25–5.0 Pa. Based on available literature data, for most large vessels,  $\overline{\tau}_{w}^{T}$ (calculated from reported mean volumetric flow rate,  $\overline{Q}$ , and vascular diameter values, d, as  $\overline{\tau}_w^T = 32\mu \overline{Q}/(\pi d^3)$ ) remains nearly constant throughout gestation, but values are reported that vary within a narrow range ( $\leq 0.25$  Pa) of values. We calculated the values of shear stress from Reymond et al. model vasculature and then scaled values for all artery segments to match available reported values at the ascending aorta, the internal common carotid artery, the common iliac, and the external iliac. We let the  $\overline{\tau}_{w}^{T}$  for all uterine artery segments follow a prescribed, nonlinear trajectory, with different target values for the low, medium, and high simulations. We let  $\overline{\tau}_{w}^{T}$  for the arcuate arteries equal 1.05-times that of the uterine artery target value and let  $\overline{\tau}_w^T$  for the radial arteries equal 1.10-times that of the uterine artery target value.

Finally, note that there are a few artery segments where shear stress regulation was not used to specify the artery diameter. First, there are several vessel segments that represent anastomoses; e.g., arcuate bridge vessels (segments 610–625) which anastomose right and left arcuate branches,

uterine artery 'bridging' vessels (segments 122–123), which are generally the stagnation point between the internal iliac-derived uterine flow and the ovarian artery-derived uterine flow. Finally, while very little data are available, it has been reported that the uterine arteries provide ~80% of the uterine blood flow during pregnancy and the ovarian arteries provide the remaining 20% (Osol and Moore 1994; Palmer et al. 1992). We defined the diameters of the ovarian arteries (segments 100–101) so that 20% of the total uterine blood flow was supplied through the ovarian artery, while the remaining 80% was supplied through the internal iliac.

### 2.2.4 Vessel wall distensibility versus gestation

Equation (5) is a useful empirical equation that arises from the observation that, in healthy, young individuals, the distensibility of arteries along the vascular tree correlates with their diameter. Therefore, Eq. (5) was used to quantify the distensibility of the non-gravid maternal vasculature. In addition to growth (e.g., changes in vessel diameter and axial length) that occurs in many arteries throughout gestation, it is likely that the distensibility also change throughout gestation. In vivo vessel wall distensibility may change due to several reasons, described below.

- 1. Strain-stiffening response. Arteries are strain stiffening materials; i.e., if a vessel distends circumferentially (e.g., to increased pressure or vasodilation) the local stiffness of the material increases due to the material nonlinearity. Similarly, if a vessel is stretch in the axial direction, the (circumferential) distensibility of the vessel decreases from this increased axial stretch. This strain stiffening response, in the circumferential and axial direction, is largely attributed to collagen fiber engagement with increasing strain. Thus, even in the absence of true remodeling (i.e., change in the material composition of the artery wall) acute changes in pressure, vasodilation, or axial length can cause a decrease in distensibility (i.e., apparent artery stiffening).
- 2. Changes in vessel wall composition. The mechanical behavior of arteries is determined by the content and organization of cells and extracellular matrix of the vessel wall. Often the ratio of collagen and elastin, two of the most predominant structural proteins in the vessel wall, is considered a key predictor of the vessel distensibility. It is now well accepted that elastin is laid down and cross-linked into a mechanically stable state early in development and maturation and, in adults, functional elastin is no longer produced in arteries (Wan and Gleason 2013). As arteries grow and remodel throughout maturity and with aging, both the elastin-to-collagen ratio and the vessel distensibility decrease and as a vessels grow in adults, growth occurs primarily through the



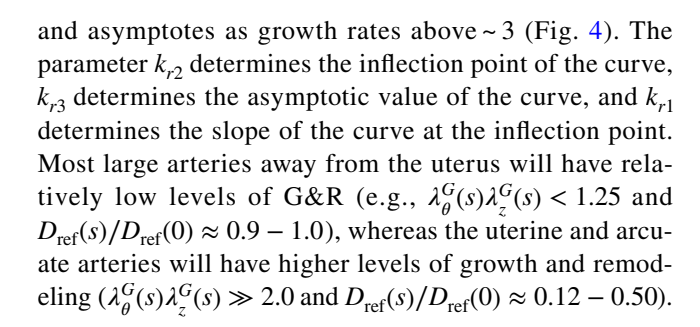
addition of 'stiffer' extracellular matrix proteins (e.g., collagen), which yields a less distensible vessel (Lakatta 2003). In humans, the elastin-to-collagen ratio also decreases with 'healthy' vascular maturity and aging and decreases to a greater degree with vascular disease (Zieman et al. 2005). While the elastin-to-collagen ratio has not been quantified in vessels from the human uterine vasculature, Woessner and Brewer showed that the total mass of collagen and elastin increased in the entire human uterus with gestational age, but that the elastinto-collagen ratio was lowest in term and 8- to 11-Day post-term uteri compared to non-gravid and 2- and 4-month post-term uteri (Woessner and Brewer 1963). If the whole uterus elastin-to-collagen ratio is related to the uterine vasculature elastin-to-collagen ratio, these data suggest that uterine arteries may become stiffer with gestation due to a decreased elastin-to-collagen ratio in the vessel wall.

3. Vessels thickening. Vessel distensibility is also determined by the vessel wall thickness; thicker vessels (or increased thickness-to-radius ratio), with similar content and organization of cells and extracellular matrix, are less distensible. Carotid artery vessel wall thickness increases significantly with age and is a key independent risk factor for cardiovascular disease (Willeit et al. 2020). Little data are available regarding changes in artery wall thickness across gestation (Anastasakis et al. 2008).

With the increased cardiac output and increase perfusion of the uterine vasculature, some vessels increase their diameter by > twofold. Further, given the increase in uterus size, vessels that transverse the uterus increase their length by 2- to 3-fold. For the gravid vascular networks, we propose a phenomenological model that relates changes in the reference distensibility to the growth of the vessels; namely,

$$D_{\text{ref}}(s) = \frac{D_{\text{ref}}(0)}{R_o} \left[ 1 + \frac{k_{r3}}{1 + \exp\left\{-k_{r1} \left(\lambda_{\theta}^G(s) \lambda_{z}^G(s) - k_{r2}\right)\right\}} \right]$$
(14)

where s denotes the gestational age,  $\lambda_{\theta}^{G}(s) = d(s)/d(s=0)$  and  $\lambda_{z}^{G}(s) = \ell(s)/\ell(s=0)$  are the fractional increases in diameter (d) and length  $(\ell)$  from the non-gravid vasculature (i.e., at s=0) and the gravid timepoint of interest, is the length of the artery segment,  $k_{r}^{1}$ ,  $k_{r}^{2}$ , and  $k_{r}^{3}$  are remodeling parameters, and  $R_{o}$  is the value of the expression in the square brackets at  $\lambda_{\theta}^{G}(s)\lambda_{z}^{G}(s)=1$ . We let  $k_{r1}=2.2$  and  $k_{r2}=1.7$  and let  $k_{r3}$  take values between -0.80 to -0.90 for different simulations. This model suggests that as a vessel grows, the ratio in  $D_{\text{ref}}(s)/D_{\text{ref}}(0)$  decreases monotonically with growth (i.e.,  $\lambda_{\theta}^{G}(s)\lambda_{z}^{G}(s)>1$ )



# 2.3 Numerical Solver and Illustrative Simulations

Numerical solver for 1D/0D fluid dynamics model. An implicit finite difference scheme was devised, following the approach of van den Boom et al., to solve the governing equations with the given vascular geometry and material properties and the governing Windkessel parameters (Supplement 1 – Implicit Finite Difference Scheme) (van den Boom et al. 2018; Kroon et al. 2012). We discretized the time domain into  $n_t = 500$  time-steps per cardiac cycle; since the heart rate changes across gestation, the time step is also slightly different for each gestational age and is given as  $dt = 60/(HR * n_t)$ . We let dz = 0.5 cm; for vessels with length segment length < 0.75 cm, we let dz = (segment)length)/2, to ensure that there are at least two elements for all vessel segments. Solutions typically converged after iterations through 5 cardiac cycles, but all results are shown for the 10<sup>th</sup> cardiac cycle.

*Illustrative simulations and G&R solving routines.* Given a prescribed time-courses of the cardiac output and target values for brachial artery mean and systolic blood pressure, blood flow distributions, uterine and ovarian blood flow rates, wall shear stresses for all vessel segments, and uterine artery pulsatility index, we iteratively solved for the terminal resistances, terminal compliances, and reference values for the diameters for each artery segment, following the logic illustrated (Fig. 5). Briefly, given that mean blood pressure and the distribution of blood flow are primarily governed by the values of the terminal resistances,  $R_T$ , we first identified the values of terminal resistances that yield the target mean brachial artery blood pressure and arterial flow rates, for which literature results are available; namely, uterine, ovarian, external iliac, renal, and internal common carotid arteries. Note that, for the external iliac, renal, and internal common carotid arteries, we calculated the ratio of the actual flow to the target literature value,  $f_{\nu}^{Q}=Q_{\nu}/Q_{\nu}^{T}$ , and iterated the code until  $f_{EI}^{Q}=f_{Renal}^{Q}=f_{ICA}^{Q}$ . After the mean blood pressure and blood flow targets are achieved, we iteratively adjusted all vessel radii until the wall shear stresses reach target values. After the pressure, flow, and shear stress targets are met, we adjusted the terminal compliances until the target uterine artery pulsatility index and systolic blood pressure (and blood pressure, blood flow, and shear stress)



Level 1: Adjust terminal resistances to match target mean flow rates in all vessels

- <u>Adjusted values</u>: Placental and non-placental radial artery  $R_T$ , ovarian artery radius and all other vessel  $R_T$  values, through prescription of  $f_L$ ,  $f_T$ , and  $f_C$ .
- <u>Targets</u>: Mean blood pressure, uterine artery and ovarian artery flow rate, ratios of external iliac, renal, and internal carotid artery flow rates to the overall cardiac output.



Level 2: Adjust reference artery diameters to match target mean shear stresses in all vessels

- Adjusted values: Reference diameters for all artery segments.
- <u>Targets</u>: Mean wall shear stress in the ascending aorta and internal common carotid, common iliac, external iliac, uterine and radial artery wall shear stresses match target values.



Level 3: Adjust terminal compliance to match uterine artery pulsatility index and systolic pressure

- <u>Adjusted values</u>: a<sub>RTC</sub> for placentally-engaged radial arteries (all radial arteries for non-gravid case) and all non-uterine terminal vessels.
- <u>Targets</u>: Uterine artery pulsatility index and systolic blood pressure.

Fig. 5 Flowchart illustrating the solver routine for the growth and remodeling the maternal vasculature during pregnancy. Terminal resistances are first iteratively adjusted until the target mean flow rates and mean arterial pressure are achieved (Level 1). Once target flow rates and mean blood pressure are achieved, reference diameters

are adjusted to achieve the target means wall shear stresses at the mid-point of each vessel segment (Level 2). When the target mean flow rates, mean blood pressure and mean wall shear stresses are achieved, the terminal compliances are adjusted to achieve the target systolic pressure and uterine artery pulsatility index (Level 3)

target values are achieved. We considered three illustrations that represented *low*, *medium*, and *high* values of cardiac output and uterine artery flow.

# 3 Results

The prescribed target hemodynamic values, the modeling parameters, the properties for the maternal vasculature, along with key values of simulation results, for each illustrative simulation, at each gestational age, are provided (Supplement 2 – Supporting Tables).

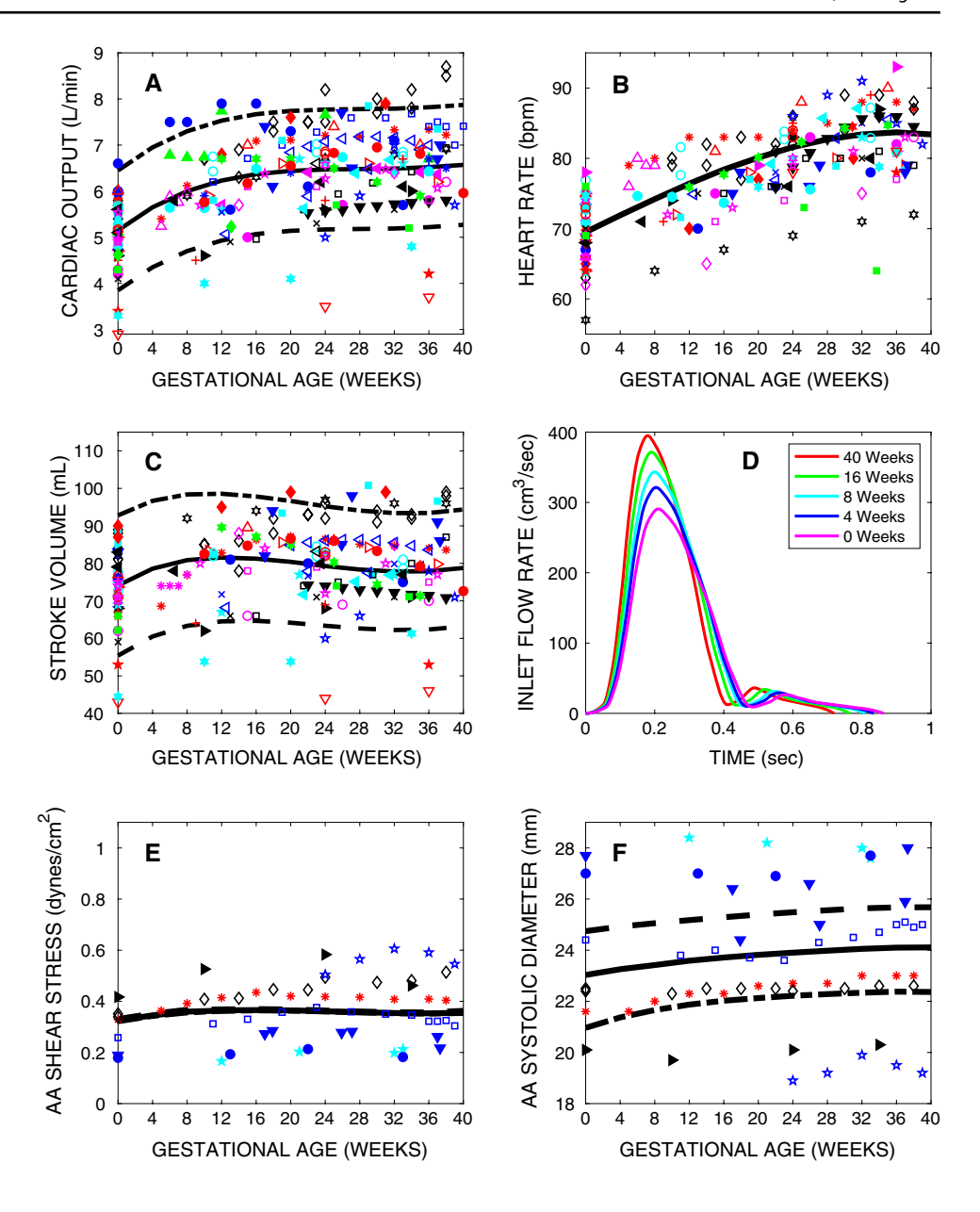
Cardiac output, heart rate, blood pressure, and total peripheral resistance. Blood pressure, cardiac output, heart rate, blood pressure and total peripheral resistance (TPR) all adapt throughout pregnancy (Figs. 6 and 7) (Clark et al. 1989; Robson et al. 1989; Easterling et al. 1990; Mabie et al. 1994; Duvekot et al. 1995; Mone et al. 1996; Hennessy et al. 1996; Clapp and Capeless 1997; Gilson et al. 1997; Geva et al. 1997; Poppas et al. 1997; Chapman et al. 1998; Wolfe et al. 1999; Mesa et al. 1999; Bosio et al. 1999; Valensise et al. 2000, 2001, 2006, 2008; Borghi et al. 2000; Del Bene et al. 2001; Schannwell et al. 2002; Simmons et al. 2002; Desai et al. 2004; Lof et al. 2005; Wilson et al. 2007; Bamfo et al. 2007a, b; Rang et al. 2007; Rang et al. 2008; Vasapollo et al. 2008; Ogueh et al. 2009; Robb et al. 2009; Hale et al. 2009; Nevo et al. 2010; Flo et al. 2010; Vlahović-Stipac et al. 2010; Kuleva et al. 2011; Dennis et al.

2012; Moertl et al. 2012; Novelli et al. 2012; Abduljalil et al. 2012; Savu et al. 2012; Estensen et al. 2012; D'Silva et al. 2013; Mahendru et al. 2014; Vårtun et al. 2014; Meah et al. 2016; Sengupta et al. 2017; Vinayagam et al. 2018; Nii et al. 2018). Cardiac output increases by 30 or 50% from conception to term in uncomplicated pregnancies, with much of the increase occurring in the first trimester. Our illustrative simulations consist of the *low*, *medium*, and *high* ranges of values reported in the literature. The increase in cardiac output occurs due to a  $\sim$  20% increase in heart rate and a 6–17% maximum increase in stroke volume. Increases in stroke volume typically occur in the first trimester, whereas increases in heart rate occur throughout gestation.

Compared to systemic hemodynamic parameters, fewer reports are available on the changes in blood flow and vessel diameter across the maternal vasculature. In the ascending aorta, despite the large increase in cardiac output through the aorta across gestation, calculated values of mean wall shear stress were remarkably uniform across gestation and across several different studies (Robson et al. 1989; Easterling et al. 1990; Mabie et al. 1994; Hennessy et al. 1996; Wolfe et al. 1999; Mesa et al. 1999; Valensise et al. 2000, 2001; Rang et al. 2007). We prescribe the shear stress in the ascending aorta and the systolic diameter of the *low*, *medium*, and *high* simulations generally followed the trends of a gradually increasing ascending aorta diameter with gestational age, consistent with literature results.



Fig. 6 Cardiac output (A), heart rate (B), stroke volume (C), aortic blood flow waveform (D), and ascending aortic shear stress (E) and ascending aortic diameter (F) versus gestational age for the Low (dashed line), Medium (solid line), and High (dash-dot line) illustrative simulations and for data reported in the literature. The legend for each mark shape, color, and fill for the literature data are provided in Supplement B



Mean, systolic, and diastolic brachial artery blood pressure generally decrease during the first trimester and increase slightly in the third trimester of pregnancy. TPR is formally defined as the difference in pressure between the aortic sinus and the peripheral venous system at the distal end of the vena cava divided by the cardiac output; however, practically, clinical studies define TPR = MAP/CO, where MAP = (SBP + 2DBP)/3, and SBP and DBP are the systolic and diastolic blood pressure measured at the brachial artery. To draw consistencies between computational modeling results and clinical data, we define TPR as done in clinical studies. In our model, TPR decreased in the first trimester and then plateaued with a modest increase toward term, which generally follows the results from the literature.

Hemodynamics and remodeling of the uterine vasculature. Uterine artery blood flow, diameter, and calculated values of  $\overline{\tau}_w^T$  show high variability across studies, compared to changes across gestation in other larger arteries (Palmer et al. 1992; Wilson et al. 2007; Flo et al. 2010; Thaler et al. 1990; Dickey et al. 1994, 1995; Dickey 1995; Dickey fand Hower 1995; Zamudio et al. 1985; Konje et al. 2001; Jeffreys et al. 2006; Browne et al. 2011) (Fig. 8). The combined volumetric blood flow through the right and left uterine arteries is ~75 ± 50 mL/min throughout the menstrual cycle and increases to ~725 ± 125 mL/min at 36 weeks, with the greatest rate of increase occurring in the second trimester. For the *low*, *medium*, and *high* simulations, we prescribed the target bilateral blood flow in the uterine arteries (segments 112 & 113) to increase



Fig. 7 Mean arterial pressure (MAP, A), systolic blood pressure (SBP, B), diastolic blood pressure (SBP, C) and total peripheral resistance (TPR, D) versus gestational age for the Low (dashed line), Medium (solid line), and High (dash-dot line) illustrative simulations and for data reported in the literature. The legend for each mark shape, color, and fill for the literature data are provided in Supplement B

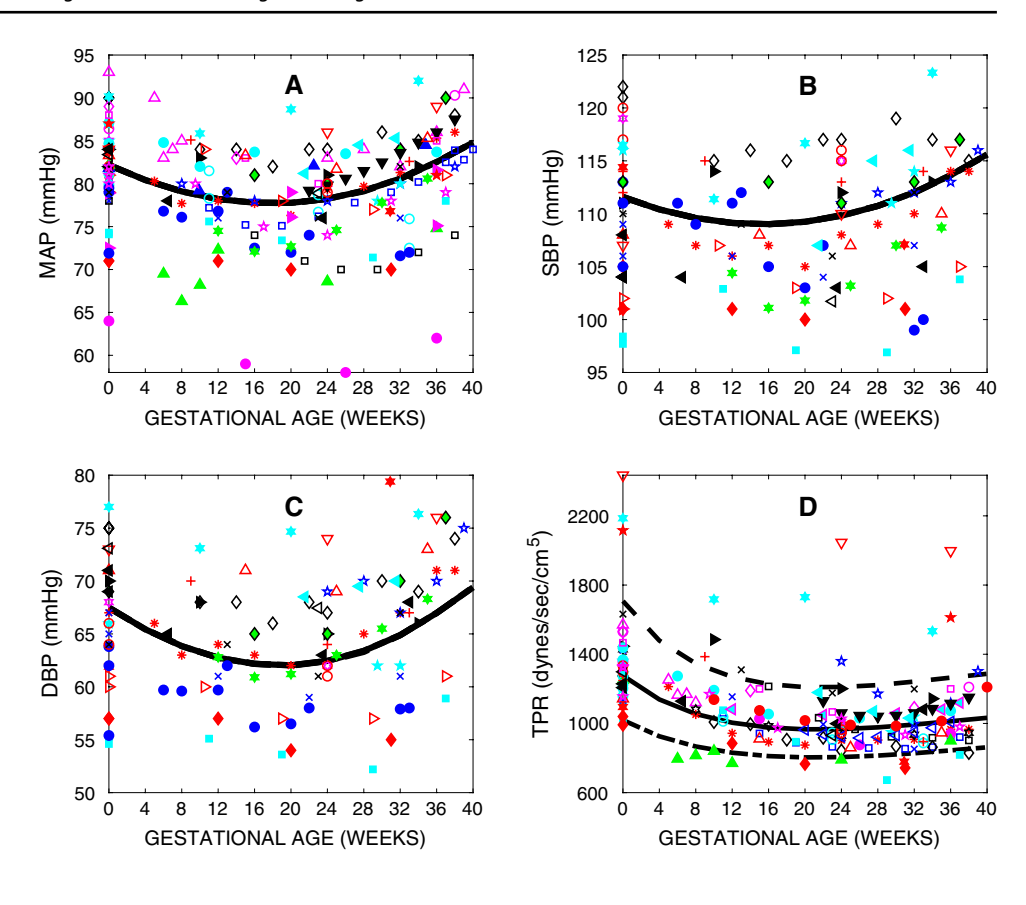
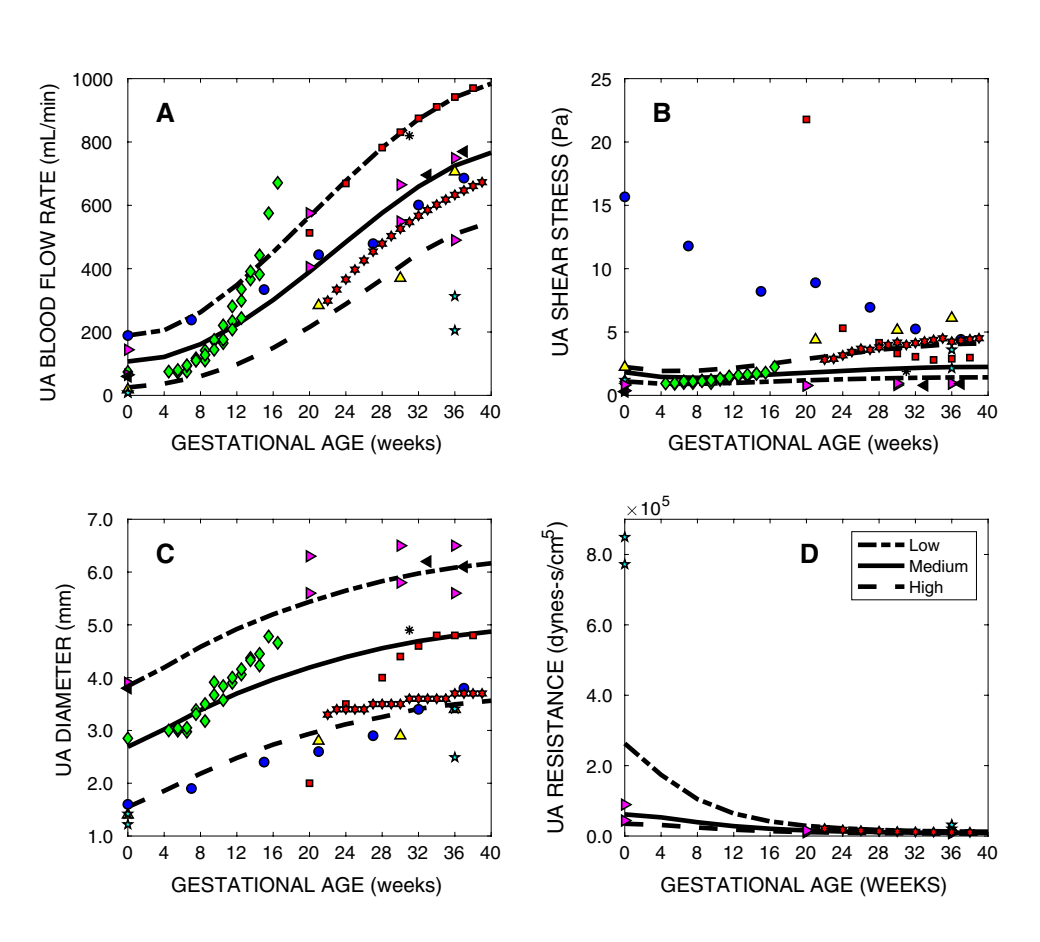


Fig. 8 Uterine artery bilateral blood flow rate (A), calculated mean wall shear stress (B), diameter (C) and peripheral resistance (D) versus gestational age for the Low (dashed line), Medium (solid line), and High (dash-dot line) illustrative simulations and for data reported in the literature. The legend for each mark shape, color, and fill for the literature data are provided in Supplement B





monotonically, but nonlinearly, from 25 to 548, from 107 to 766, and from 189 to 984 mL/min, respectively, from 0 to 40 weeks of gestation, which represent a 22-, 7.2-, and 5.2-fold increases in flow, respectively. A broad range of values for uterine diameter have been reported, ranging from 1.4 to 3.9 mm in non-gravid women and from 3.4 to 6.5 mm at 36 weeks of gestation. The uterine artery wall shear stresses, calculated based on reported values of diameter and blood flow, also show a very high degree of variability across studies and across gestation. The target values for the *low*, *medium*, and *high* simulations, combined with the prescribed blood flow, yield uterine artery diameter values that span the range of reported values and represent a 1.6-, 1.8-, and 2.3-fold increases in diameter for the *low*, *medium*, and *high* simulations.

The peripheral resistance of the uterine vasculature,  $PR_{UA} = MAP/Q_{UA}$ , where  $Q_{UA}$  is the bilateral uterine flow reduced dramatically in the first trimester, then more gradually during the second and third trimester; modeling results capture well the observed values from the literature. The reduction in  $PR_{UA}$  is attributed primarily to the reduction in the values of  $R_T$  for the placentally engaged radial arteries, which led to a 87-, 26-, and 18-fold increase in flow and (to restore the target shear stress) a 3.6-, 2.8-, and 2.4-fold increase in the diameter of the placentally engaged radial arteries for the *low*, *medium*, and *high* simulations,

respectively. Similarly, the first arcuate artery branches, at the level of the center of the placenta, show 68-, 20-, and 14-fold increases in flow and 3.4-, 2.6-, and 2.2-fold increases in diameter for the *low*, *medium*, and *high* simulations.

The flow through the ovarian arteries was prescribed to be 20% of the entire blood flow to the uterine vasculature (Fig. 9). This flow was governed by adjusting the ovarian artery diameter to achieve the target flowrate. The shear stress of the ovarian arteries that resulted from the solved values of diameter was 3.5- to 5-times higher than the shear stress prescribed in the uterine arteries. Remarkably, the ratio of shear stress in the ovarian artery to that in the uterine artery was very consistent across the *low*, *medium*, and *high* simulations and only increased slightly with gestation.

The shape of the uterine artery centerline blood velocity resembled well those reported in the literature (Gómez et al. 2008; Sciscione et al. 2009) (Fig. 10). Experimental results across a large number of studies suggest that metrics characterizing the shape of the Doppler ultrasound-measured centerline velocity profile in the uterine artery over the cardiac cycle changes dramatically throughout gestation; while changes across gestation are large, the time-course of these values is tightly conserveed across studies from multiple continents and people groups (Wilson et al. 2007; Dickey et al. 1994; Browne et al. 2011; Gómez et al. 2008, 2005;

**Fig. 9** Ovarian artery bilateral blood flow rate (**A**), wall shear stress (**B**), diameter (**C**), and peripheral resistance (**D**) for the low, medium, and high simulation

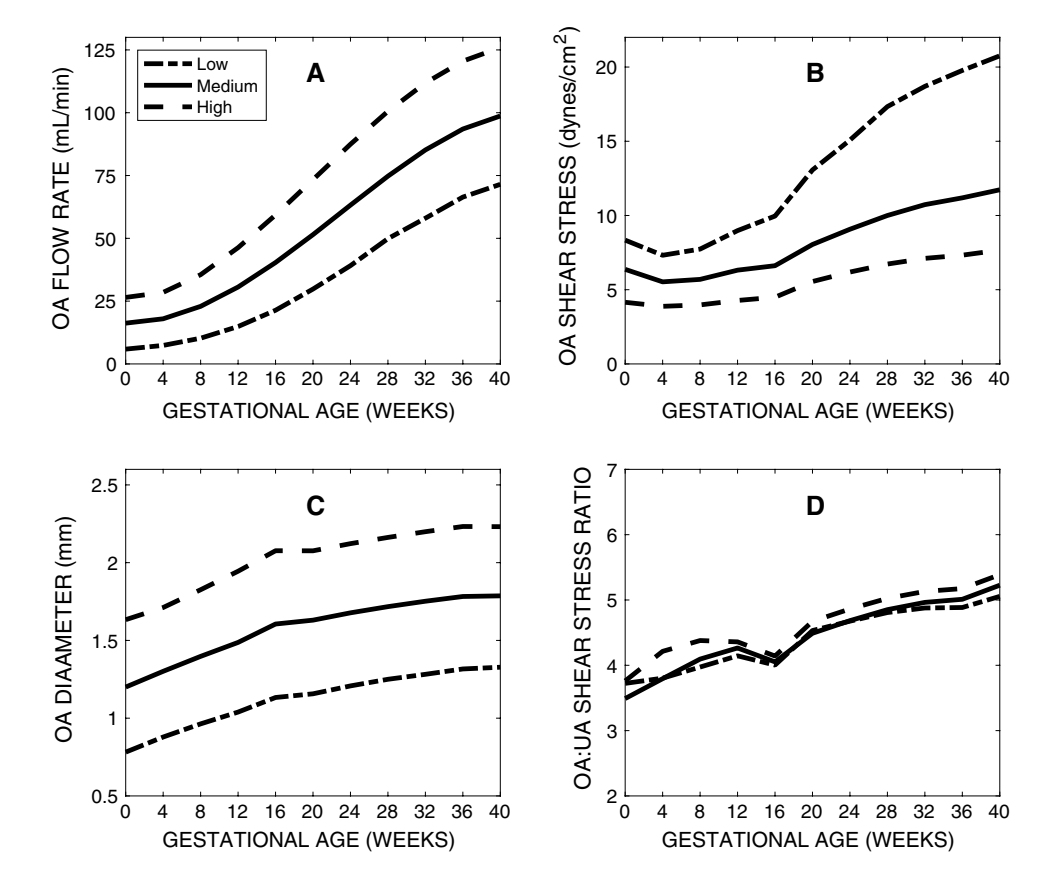
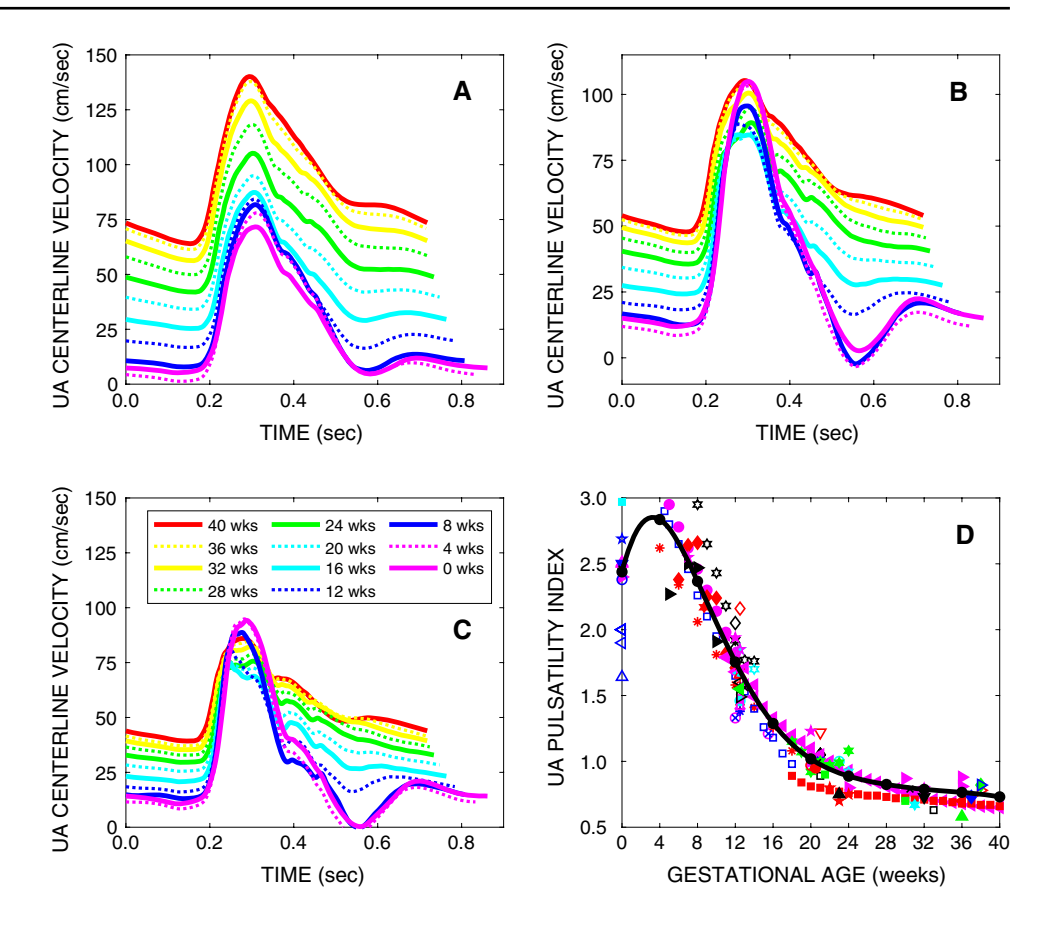




Fig. 10 Uterine artery centerline blood flow velocity profiles over one cardiac cycle for Low (A), Medium (B), and High (C) illustrative simulations for each gestational age considered from 0 to 40 weeks. Notice the presence of the early diastolic notch in the first trimester, but not in the second and third trimester waveforms Uterine artery pulsatility index (UA-PI) versus gestational age (D) for the illustrative simulations (Low, Medium, and High, solid line) and for data reported in the literature. The legend for each mark shape, color, and fill for the literature data are provided in Supplement B



Deutinger et al. 1988; Jurkovic et al. 1991; Jauniaux et al. 1991; Kaminopetros et al. 1991; Fugino et al. 1993; Olofsson et al. 1993; Coppens et al. 1996; Valentin et al. 1996; Tekay et al. 1996; Guanes et al. 1996; Sagol et al. 1999; Yalti et al. 2003; Mäkikallio et al. 2004; Pilalis et al. 2007; Ozkaya et al. 2007; Yu et al. 2008; Poon et al. 2009a, b; Deurloo et al. 2009; Rigano et al. 2010; Audibert et al. 2010; Wang et al. 2010; Odibo et al. 2011; Eser et al. 2011; Farina et al. 2011; Bahlmann et al. 1980; Everett et al. 2012; Lai et al. 2013; Arcangeli et al. 2013; Scazzocchio et al. 2013; Prajapati and Maitra 2013; Jamal et al. 2013; Paco et al. 2014; Oliveira et al. 2014; Guedes-Martins et al. 2014; Ergin and Yayla 2015; Crovetto et al. 2015; Borna and Rahmani 2015; Carter et al. 2015; Plasencia et al. 2015; Khalil et al. 2016; García et al. 2016; Kienast et al. 2016; Tezcan et al. 2015; Cheng et al. 2015; Kumar et al. 2016; Abdel Moety et al. 2016; Zebitay et al. 2016; Leite et al. 2019; Cavoretto et al. 2020; Ponmozhi et al. 2019; Perry et al. 2020; Prodan et al. 2019; D'Antonio et al. 2020; Adekanmi et al. 2019).  $UA-PI = (v_{PS} - v_{ED})/\overline{v}$  has emerged as a reliable indicator of peripheral resistance of the uterine vasculature and early indicator of risk of preeclampsia and fetal growth restriction, where  $v_{PS}$  is the peak systolic centerline velocity,  $v_{ED}$  is the end diastolic centerline velocity, and  $\overline{v}$  is the time-averaged mean centerline velocity of the uterine artery, usually taken in the ascending branch of the uterine arterey at level of the cervical os or near the intersection point of the uterine artery and the external iliac artery.

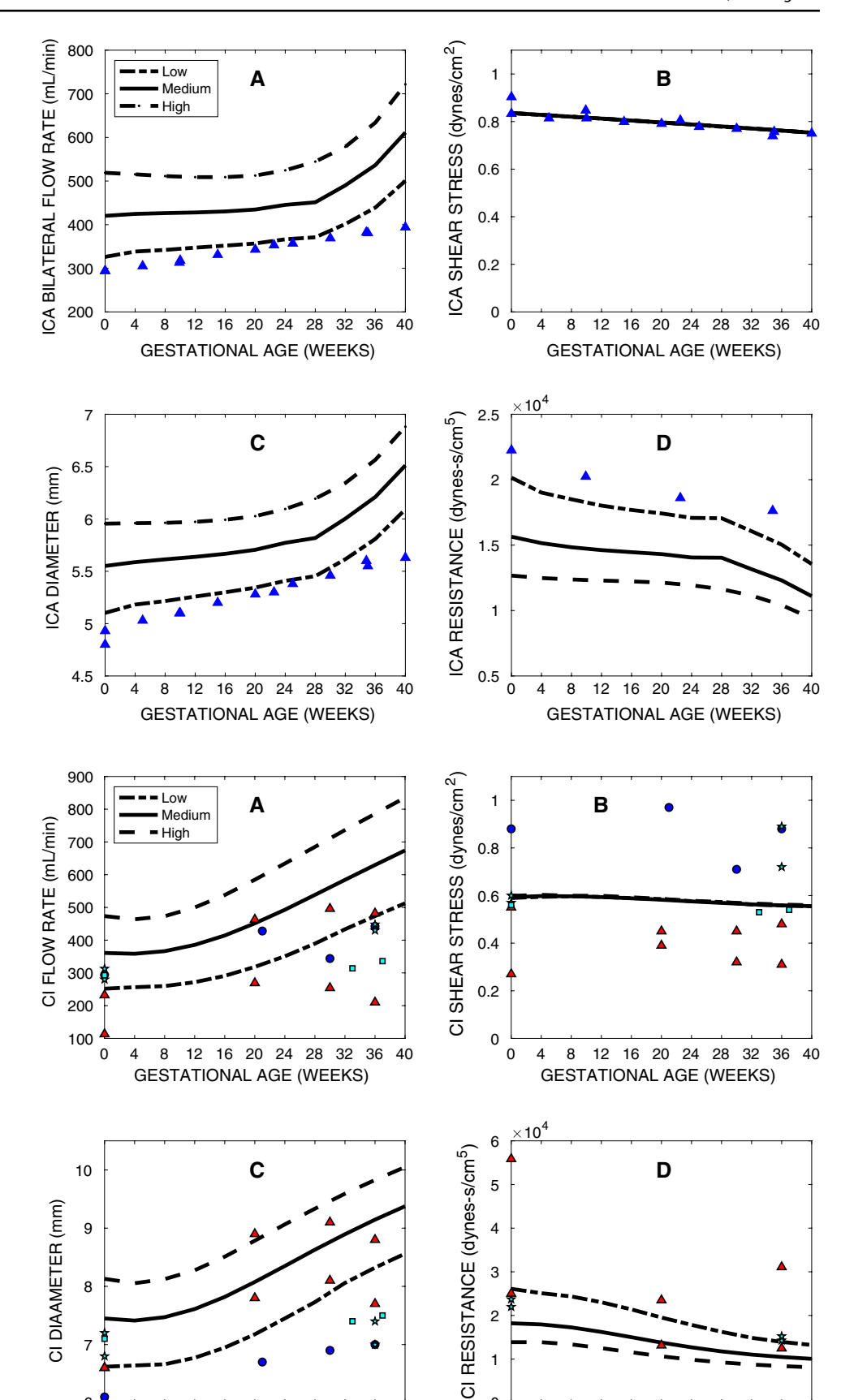
Hemodynamics and remodeling of other non-uterine vasculature. A few studies are available for blood flow in the internal carotid (Nevo et al. 2010), renal (Abduljalil et al. 2012), and common iliac and external iliac (Palmer et al. 1992; Wilson et al. 2007; Zamudio et al. 1985; Browne et al. 2011) arteries. In general, our low computational modeling simulations most closely capture the reported flows and diameters of these published results (Figs. 11, 12, 13); the medium and high simulations show higher flow and diameter values. Nevo et al., 2010 reported changes in the ICA across gestation and calculated values of shear stress, using their results, showed a nearly constant shear stress across gestation. Reported values of renal blood flow increase from ~880 to ~1330 mL/min from 0 to 20 weeks and then decrease back toward ~ 900 mL/min at term. No diameter data were reported for the renal arteries, so shear stress calculations and diameter comparisons were not available. Blood flow in the common iliac artery increases, primarily due to increases in the uterine blood flow. Note that the studies that report common iliac blood flow rates generally report lower than average values of uterine artery flow rates; while the nominal calculated values of shear stress in common iliac arteries vary between 0.2 and 1.0 dynes/cm<sup>2</sup>, all studies show that the



12 16 20 24 28 32 36 40

GESTATIONAL AGE (WEEKS)

Fig. 11 Internal carotid artery (ICA) bilateral blood flow rate (A), wall shear stress (B), diameter (C), and peripheral resistance (D) for the low, medium, and high simulation and the results from Nevo et al. (2010) (blue triangles)



12

16 20 24 28

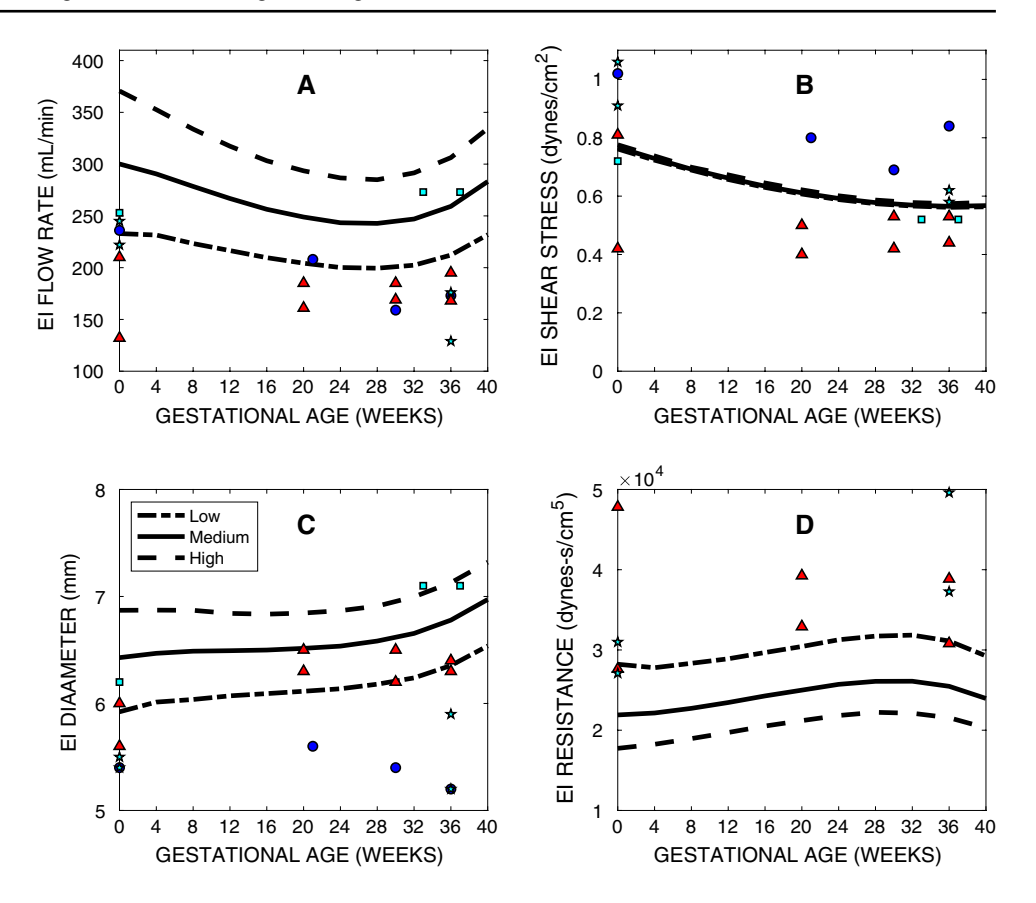
**GESTATIONAL AGE (WEEKS)** 

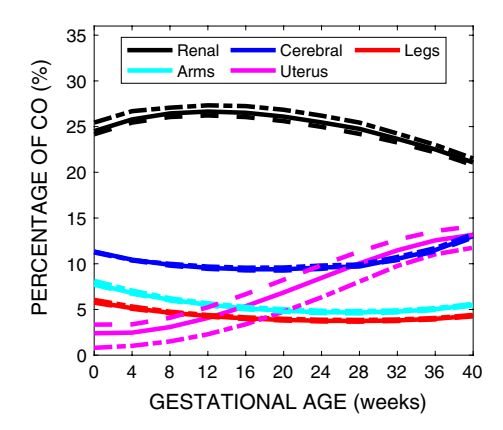
32 36 40

Fig. 12 Common iliac blood flow rate (A), wall shear stress (B), diameter (C), and peripheral resistance (D) for the low, medium, and high simulation and the results from Palmer et al. (1992) (blue circles), Zamudio et al. (1985) (cyan stars), Wilson et al. (2007) (red triangles), and Browne et al. (2011) (cyan squares)



Fig. 13 External iliac blood flow rate (A), wall shear stress (B), diameter (C), and peripheral resistance (D) for the *low*, *medium*, and *high* simulation and the results from Palmer et al., 1992 (blue circles), Zamudio et al., 1995 (cyan stars), Wilson et al., 2007 (red triangles), and Browne et al., s 2011 (cyan squares) (Palmer et al. 1992; Wilson et al. 2007; Zamudio et al. 1985; Browne et al. 2011)





**Fig. 14** Blood flow perfusion rates of the renal, cerebral, leg, arm, and uterine vasculature versus gestational age presented as a percentage of the total cardiac output. The low, medium, and high simulation results are presented as the dash-dot, solid, and dashed lines, respectively, for each vascular bed

shear stress in the common iliac remains nearly constant throughout gestation. A gap also remains in the literature describing the time course of changes in perfusion differ in different vascular beds, as a fraction of total cardiac output. In our model, the combined uterine and ovarian flow comprising of 0.8–3.3% of the total CO at conception to 12–14% at term (Fig. 14). The renal perfusion varies from

20–27% of the total CO, initially increasing in the first trimester, then decreasing in the second and third trimester. Cerebral perfusion varies from 9–13% of total CO, initially decreasing, then increasing in the third trimester. Perfusion of the arms and legs decreases in the first trimester and then remains nearly constant.

Changes in vessel distensibility. Pulse wave velocity (PWV) has emerged as a useful surrogate clinical metric to assess large artery stiffness and vascular age, with carotid-femoral (cf) PWV considered the gold standard metric (Laurent et al. 2019). Numerous methods have been used to assess central arterial stiffness in pregnancy in pregnancy, including cf-PWV (Anastasakis et al. 2008; Rang et al. 2007; Robb et al. 2009; Mahendru et al. 2014, 2017; Savvidou et al. 2011; Kaihura et al. 2009; Graaf et al. 2008), radial-femoral (rf) PWV (Robb et al. 2009; Savvidou et al. 2011; Kaihura et al. 2009), brachial-ankle PWV (Oyama-Kato et al. 2006), and augmentation index (Robb et al. 2009; Mahendru et al. 2014, 2017; Savvidou et al. 2011; Kaihura et al. 2009; Graaf et al. 2008). Our computational modeling results show a slight decrease in cf PWV and crPWV in the first half of pregnancy, then an increase in these values in the second half of pregnancy (Fig. 15). Cyclic strain, defined as  $\Delta \varepsilon = (d_{sys} - d_{dias})/\overline{d}$ , decreases over the first trimester in arcuate arteries and over the first half of pregnancy for uterine arteries, asymptotically to values < 1%; this is because the arcuate and uterine arteries experience large



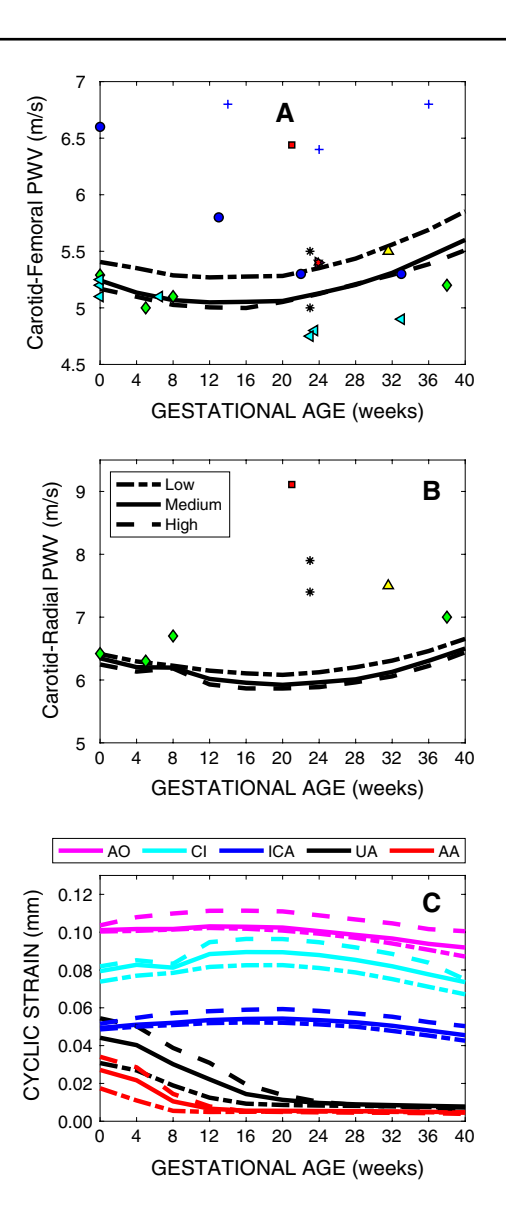


**Fig. 15** Carotid-femoral pulse wave velocity (PWV, **A**), carotid-radial PWV (**B**) and cyclic strain for the aorta (AO), common iliac (CI), internal carotid artery (ICA), uterine artery (UA) and arcuate artery (AA, **C**) for Low, Medium, and High illustrative simulations for each gestational age considered from 0 to 40 weeks. The legend for each mark shape, color, and fill for the literature data are provided in Supplement B

circumferential growth  $(\lambda_{\theta}^G)$  due to large increases in flow and shear stress-mediated remodeling and large axial growth  $(\lambda_z^G)$  associated with the dramatic growing uterus. Non-uterine arteries do not grow axially and experience only modest circumferential growth. Cyclic strain in non-uterine arteries generally increases in the first half of pregnancy and then decreases in the second half of pregnancy.



Adequate G&R of the maternal vasculature, coupled with increased cardiac output, are essential events to provide adequate blood flow to the placenta during pregnancy. The uterine vasculature experiences the greatest amount of G&R. Vascular G&R is initiated early in the first trimester, as extravillous trophoblasts form a plug in the spiral arteries and distal regions of the radial arteries, preventing blood flow into the intravillous space. The trophoblasts replace spiral artery endothelial cells and smooth muscle cells, transforming the spiral arteries from high resistance vasoactive arterioles to low resistance passive conduits after the resolution of the plug (Osol and Moore 1994; Osol and Mandala 2009; James et al. 2017; Brosens et al. 2002). Plugging of the spiral arteries may also stimulate the formation of A-V shunts between radial arteries and radial veins across the upper half of the myometrium (Burton et al. 2009). If present, the A-V shunts would significantly reduce uterine peripheral resistance in the first 10 weeks, prior to increased blood flow to the intravillous space—increasing blood flow through the uterine, arcuate, and radial arteries and distal myometrial and uterine veins-initiating flow-mediated G&R in these vessels, and perhaps 'preparing' these vessels for the rapid increase in flow that will be required in the second and third trimester. The spiral artery plugs begin to resolve at approximately 8 weeks and become fully resolved by 12 weeks of gestation, allowing blood flow to the intravillous space. In our model, spiral artery remodeling and A-V shunt formation are collectively captured by the WK3 model at the termination of each of the 60 placentally engaged radial arteries. Target values of blood flow, which span the range of values reported in the literature, were used to iteratively solve for the WK3 resistances in placentally engaged radial arteries. To achieve the target values of uterine flow, there was a dramatic reduction it the total resistance  $(R_T)$ of the placentally engaged radial arteries, with the greatest decrease occurring in the first four weeks, when the spiral arteries are plugged, suggesting that nearly all the flow must travel through the A-V shunts.

We also prescribed changes in  $R_T$  in the leg, arm, trunk, and cerebral vasculature throughout gestation to, as best as posible, capture the changes in blood flow and diameter in the internal carotid artery, common and external iliacs, and renal artery. No reports measured flow in different regions of the body, in the same cohort of subjects; pelvic vessel data, ICA data, and renal data all from different papers and these reports often did not report total cardiac output. It seems that the available reports correlate most closely with our *low* simulation. Adjustments in the assumed changes in blood flow throughout the vasculature had a significant effect on uterine perfusion and parameters such as UA-PI (results not shown);



there is a need to perform parametric studies to quantify the role of blood flow distribution throughout the body on placental perfusion. There is also a pressing need to quantify, in the same subjects, how blood flow and peripheral resistances in each vascular bed change throughout gestation. Indeed, developing subject-specific models, validated with data from individual subjects across gestation, for both normal pregnancies and pregnancies complicated with preeclampsia and fetal growth restriction could help to reveal the interplay of the milieu of hemodynamic and vascular changes.

Following the adjustment of the  $R_T$  values for all the terminal vascular segments to match the target flow rates, vessel growth was prescribed by iteratively adjusting the vessel diameter (while continuing to adjust  $R_T$ ) to restore wall shear stress (while also continuing to match target flow rates). While results from the literature are limited, calculated shear stress values from the ascending aorta, internal carotid artery, and common iliac suggest that, despite significant changes in flow and diameter, wall shear stress remains nearly constant in these vessels across gestation, while some studies show a modest decrease in wall shear stress in the external iliac artery with gestational age. In contrast, the literature reports of shear stress values in the uterine artery are less consistent, with different studies reporting order-ofmagnitude differences in shear stress values. Some studies show uterine artery shear stress decreasing with gestation, others show it increasing, and still others show it to be constant. This variability may be due, in part, to incomplete remodeling of the uterine vasculature to the very large increases in diameter and blood flow through this vasculature. The variability in diameter and shear stress values may also be due to the redundancies in the uterine blood supply; i.e., the ovarian and internal iliac blood supply redundancy and the right-to-left redundancies in blood supply.

Our modeling results also revealed that, to constrain the ovarian flow to 20% of the total perfusion of the uterine vasculature, the ovarian artery wall shear stress was 3.5- to 5-times higher than the uterine arteries and that this ratio was fairly well conserved across the fairly broad set of uterine perfusions and cardiac outputs represented by the *low*, medium, and high simulations. Very few studies were found that quantified ovarian flow across gestation, likely because the ovarian arteries are difficult to access with ultrasound as the uterus grows. Subtle changes in the percentage of flow had significant effects on the shape of the uterine artery centerline blood flow velocity waveforms, and therefore metrics like UA-PI (results not shown). The proportion of blood flow to the uterus that arises from the ovarian artery versus the uterine artery is ultimately controlled by the differential vascular G&R between the different pathways. Thus, there is a pressing need to better understand the role ovarian artery growth may have on perfusion of the uterine vasculature and hemodynamic indicators used to assess pregnancy risk,

using both novel experimental measurements and computational models.

In addition to growth (i.e., changes in vascular caliber and length), we also prescribed remodeling (i.e., changes in vessel distensibility) to correlate with changes in vessel diameter and length via Eq. (10). By far, the largest decreases in vessel distensibility occurred in the uterine and arcuate arteries, which experienced large growth; both circumferential growth  $(\lambda_a^G)$  and axial growth  $(\lambda_z^G)$ . We found that the reduction in distensibility was necessary to achieve the target values of UA-PI and that these changes resulted in a significant reduction in cyclic strain in the uterine and arcuate arteries. Little data are available on the distensibility or cyclic strain of the uterine vasculature, like because cyclic strains are < 2% for much of gestation; it is difficult to detect these small diameter changes with ultrasound. The remaining vasculature showed only modest changes in distensibility. Changes in cyclic strain result from changes in vessel geometry (e.g., increased diameter), applied loads (e.g., change in systolic and diastolic blood pressure), and material properties (e.g., vessel distensibility). Very few direct measurements of cyclic strain are available; however, Rang et al. showed a decrease in cyclic strain of the ascending aorta from 12 weeks (8.0%) to 22 (6.3%) and 33 (6.5%) weeks and post-partum (6.3%) in uncomplicated pregnancies (Rang et al. 2007).

Following the adjustment of the  $R_T$  values and vessel diameters to match blood flow rates and wall shear stresses, the terminal compliances were iteratively adjusted to match the uterine artery pulsatility index and the systolic blood pressure. Given that UA-PI has emerged as an important prognostic indicator of pregnancy complications (e.g., fetal growth restriction and preeclampsia), perhaps more than any other parameter, we emphasized matching the shape of the uterine artery centerline velocity waveform and the UA-PI to the literature reports. Importantly, while the radial artery terminal compliance values were used to achieve target values, many other parameters played a role in reaching these targets, including the shear stress target values, the remodeling parameters, the shape of the inlet flow waveforms, among many others.

In addition to *UA-PI*, several other features of this waveform have been reported, with which we can compare our computational results. The trends in  $v_{PS}$  differ in the three illustrative simulations. In the *low* simulation,  $v_{PS}$  increased from 67 cm/s to 144 cm/s from 0 to 40 weeks of gestation. In the *medium* and *high* simulations, changes in  $v_{PS}$  were much lower. Few reports are available, but some suggest that values of  $v_{PS}$  generally increase with gestation from ~40 cm/s in non-gravid women to ~140 cm/s by 18 weeks of gestation (Jauniaux et al. 1991; Valentin et al. 1996), which are consistent with the *low* simulation. Other reports suggest more modest increases in  $v_{PS}$  from ~45 cm/s to 84 cm/s



(Wilson et al. 2007; Adekanmi et al. 2019), consistent with the *medium* and *high* simulations. Most reports in the literature show a fairly uniform increase in end diastolic velocity that corroborates the increase in perfusion. Our velocity waveforms are also consistent with most studies which show the presence of an early diastolic notch in the first trimester that goes away early in the second trimester (Gómez et al. 2008; Sciscione et al. 2009). This early diastolic notch is an important feature of these velocity waveform given that the presence of the early diastolic notch at 12–14 weeks of gestation is considered a risk factor for later development of preeclampsia and other complications. Taken together, our illustrative simulations capture well the blood flow through the uterine artery and capture seemingly discordant results from the literature.

While these computational modeling results were validated, as best as possible, with experimental results from the literature, this study has several key limitations. First, while many data sets were available and this modeling framework helps highlight critical gaps in available experimental data, give the lack of certain data, rather bold assumptions were made regarding the uterine vascular network. We assumed eight, non-branching arcuate arteries exist in each uterus quadrant that, together, feed 120 radial arteries. We assumed values of arcuate and uterine artery tortuosity. While these assumptions were based on our 'best guesses' from a small number of studies or accepted paradigms, to the best of our knowledge, these parameters are not rigorously quantified and reported. We assumed that all the placentally engaged radial arteries (and similarly all the non-placentally engaged radial arteries) have common diameters and WK3 parameteres. It is more likely that these values take a range of values across all radial arteries, but no data are available to inform these decisions. There is a pressing need to experimentaly quantify the connectivity of the uterine vascular network, vessel lengths and tortuosity, and vascular calibers of each segment and how these parameters changes across individuals, populations, and with different pregnancy complications. As imaging modalities continue to improve, this should be an important research target.

Another limitation of this study is that the data to which the computational modeling results were compared were taken from a broad range of studies; no one study comprised most or all of the measurements required to properly validate these computational modeling results. While this is a noted limitation, this limitation highlights the need for patient-specific, comprehensive data sets that quantify changes in cardiac function, vessel geometry, mechanical properties, and blood flow rates, and blood pressure pulse waveformes at multiple locations along the vasculature, a more accurate assessment of the uterine vascular network, including numbers of arcuate, radial, and spiral arteries, and tortuosity of uterine and arcuate arteries, and accurate quantification of

placental size, location, and number and size of radial arteries that communicate to the placenta. Finally, while many assumptions were made regarding these values, another limitation of this study is that only a few illustrative simulations were performed. With unmet data needs computational models provide a useful tool to quantify the impact of inaccurate assumptions, through parametric studies; the need for these studies remains.

In closure, this paper presents a mathematical framework to characterize maternal vascular G&R and hemodynamics in uncomplicated human pregnancies. Our results captured well the time-course of vessel geometry, material properties, and hemodynamics across a broad range of clinical reports and across gestation. While results capture available data well, this study highlights significant gaps in available data required to better understand vascular remodeling in pregnancy.

Supplementary Information The online version contains supplementary material available at https://doi.org/10.1007/s10237-021-01555-0.

**Acknowledgements** We gratefully acknowledge the support from the US National Science Foundation (CMMI 1727573).

#### **Declarations**

**Conflict of interest** The authors have no conflicts of interest to declare.

# References

Abdel Moety GAF, Almohamady M, Sherif NA, Raslana AN, Mohamed TF, El Moneam HMA et al (2016) Could first-trimester assessment of placental functions predict preeclampsia and intrauterine growth restriction? A prospective cohort study. J Matern Fetal Neonatal Med 29(3):413–417

Abduljalil K, Furness P, Johnson TN, Rostami-Hodjegan A, Soltani H (2012) Anatomical, physiological and metabolic changes with gestational age during normal pregnancy: a database for parameters required in physiologically based pharmacokinetic modelling. Clin Pharmacokinet 51(6):365–396

Adekanmi AJ, Roberts A, Akinmoladun JA, Adeyinka AO (2019) Uterine and umbilical artery doppler in women with preeclampsia and their pregnancy outcomes. Niger Postgrad Med J 26(2):106–112

Anastasakis E, Paraskevas KI, Papantoniou N, Daskalakis G, Mesogitis S, Mikhailidis DP et al (2008) Association between abnormal uterine artery Doppler flow velocimetry, risk of preeclampsia, and indices of arterial structure and function: a pilot study. Angiology 59(4):493–499

Arcangeli T, Giorgetta F, Farina A, De Musso F, Bellussi F, Salsi G et al (2013) Significance of uteroplacental Doppler at midtrimester in patients with favourable obstetric history. J Matern Fetal Neonatal Med 26(3):299–302

Audibert F, Boucoiran I, An N, Aleksandrov N, Delvin E, Bujold E et al (2010) Screening for preeclampsia using first-trimester serum markers and uterine artery Doppler in nulliparous women. Am J Obstet Gynecol. 203(4):383.el-383.e8



- Bahlmann F, Fittschen M, Reinhard I, Wellek S, Steiner E (2012) Reference values for blood flow velocity in the uterine artery in normal pregnancies from 18 weeks to 42 weeks of gestation calculated by automatic Doppler waveform analysis. Ultraschall in der Medizin (Stuttgart, Germany: 1980) 33(3):258–64
- Bamfo JEAK, Kametas NA, Chambers JB, Nicolaides KH (2007a) Maternal cardiac function in fetal growth-restricted and nongrowth-restricted small-for-gestational age pregnancies. Ultrasound Obstet Gynecol 29(1):51–57
- Bamfo JEAK, Kametas NA, Nicolaides KH, Chambers JB (2007b) Maternal left ventricular diastolic and systolic long-axis function during normal pregnancy. Eur J Echocardiogr 8(5):360–368
- Boileau E, Nithiarasu P, Blanco PJ, Müller LO, Fossan FE, Hellevik LR et al (2015) A benchmark study of numerical schemes for one-dimensional arterial blood flow modelling. Int J Numer Methods Biomed Eng 31(10):e02732
- Borghi C, Esposti DD, Immordino V, Cassani A, Boschi S, Bovicelli L et al (2000) Relationship of systemic hemodynamics, left ventricular structure and function, and plasma natriuretic peptide concentrations during pregnancy complicated by preeclampsia. Am J Obstet Gynecol 183(1):140–147
- Borna S, Rahmani Z (2015) A Study of Doppler ultrasound indices of spiral placental and umbilical arteries in pregnant women with singlet on pregnancy suffering type-1 diabetes mellitus, gestational diabetes and normal pregnant women. J Appl Environ Biol Sci 5(10S):436–440
- Bosio PM, McKenna PJ, Conroy R, O'Herlihy C (1999) Maternal central hemodynamics in hypertensive disorders of pregnancy. Obstet Gynecol 94(6):978
- Brosens I (1964) A study of the spiral arteries of the decidua Basalis in normotensive and hypertensive pregnancies. BJOG Int J Obstet Gynaecol 71(2):222–230
- Brosens I, Dixon HG (1966) The anatomy of the maternal side of the placenta. J Obstet Gynaecol Br Commonw 73(3):357–363
- Brosens I, Robertson WB, Dixon HG (1967) The physiological response of the vessels of the placental bed to normal pregnancy. J Pathol Bacteriol 93(2):569–579
- Brosens JJ, Pijnenborg R, Brosens IA (2002) The myometrial junctional zone spiral arteries in normal and abnormal pregnancies: a review of the literature. Am J Obstet Gynecol 187(5):1416–1423
- Brosens I, Pijnenborg R, Vercruysse L, Romero R (2011) The "Great Obstetrical Syndromes" are associated with disorders of deep placentation. Am J Obstet Gynecol 204(3):193–201
- Browne VA, Toledo-Jaldin L, Davila RD, Lopez LP, Yamashiro H, Cioffi-Ragan D et al (2011) High-end arteriolar resistance limits uterine artery blood flow and restricts fetal growth in preeclampsia and gestational hypertension at high altitude. Am J Physiol Regul Integr Comp Physiol 300(5):R1221–R1229
- Burton GJ, Woods AW, Jauniaux E, Kingdom JCP (2009) Rheological and physiological consequences of conversion of the maternal spiral arteries for uteroplacental blood flow during human pregnancy. Placenta 30(6):473–482
- Carson J, Warrander L, Johnstone E, van Loon R (2019) Personalising cardiovascular network models in pregnancy: a two-tiered parameter estimation approach. Int J Numer Method Biomed Eng. 37:e3267
- Carter EB, Goetzinger K, Tuuli MG, Odibo L, Cahill AG, Macones GA et al (2015) Evaluating the optimal definition of abnormal first-trimester uterine artery doppler parameters to predict adverse pregnancy outcomes. J Ultrasound Med Off J Am Inst Ultrasound Med 34(7):1265–1269
- Cavoretto P, Farina A, Gaeta G, Sigismondi C, Spinillo S, Casiero D, et al. Longitudinal cohort study of uterine artery Doppler in singleton pregnancies obtained by IVF/ICSI with fresh or frozen

- blastocyst transfers in relation to pregnancy outcomes. Ultrasound Obstet Gynecol. 2020:21969.
- Chapman AB, Abraham WT, Zamudio S, Coffin C, Merouani A, Young D et al (1998) Temporal relationships between hormonal and hemodynamic changes in early human pregnancy. Kidney Int 54(6):2056–2063
- Chen C, Huang R, Liu P, Ouyang Z, Guo H, Tang L et al (2010) Construction and clinical significance of normal uterine arterial vascular network models. Gynecol Obstet Invest 69(1):14–19
- Cheng F, Li T, Wang Q-L, Zhou H-L, Duan L, Cai X (2015) Effects of hydrosalpinx on ultrasonographic parameters for endometrial receptivity during the window of implantation measured by power color Doppler ultrasound. Int J Clin Exp Med 8(4):6103–6108
- Clapp MJF III, Capeless MDE (1997) Cardiovascular function before, during, and after the first and subsequent pregnancies. Am J Cardiol 80(11):1469–1473
- Clark SL, Cotton DB, Lee W, Bishop C, Hill T, Southwick J et al (1989) Central hemodynamic assessment of normal term pregnancy. Am J Obstet Gynecol 161(6 Pt 1):1439–1442
- Clark AR, James JL, Stevenson GN, Collins SL (2018) Understanding abnormal uterine artery Doppler waveforms: A novel computational model to explore potential causes within the utero-placental vasculature. Placenta 66:74–81
- Coppens M, Loquet P, Kollen M, DeNeubourg F, Buytaert P (1996) Longitudinal evaluation of uteroplacental and umbilical blood flow changes in normal early pregnancy. Ultrasound Obstet Gynecol Off J Int Soc Ultrasound Obstet Gynecol 7(2):114–121
- Corsini C, Cervi E, Migliavacca F, Schievano S, Hsia T-Y, Pennati G (2017) Mathematical modelling of the maternal cardiovascular system in the three stages of pregnancy. Med Eng Phys 47:55–63
- Crovetto F, Figueras F, Triunfo S, Crispi F, Rodriguez-Sureda V, Dominguez C et al (2015) First trimester screening for early and late preeclampsia based on maternal characteristics, biophysical parameters, and angiogenic factors. Prenat Diagn 35(2):183–191
- D'Antonio F, Rizzo G, Gustapane S, Buca D, Flacco ME, Martellucci C et al (2020) Diagnostic accuracy of Doppler ultrasound in predicting perinatal outcome in pregnancies at term: a prospective longitudinal study. Acta Obstet Gynecol Scand 99(1):42–47
- D'Silva LA, Davies RE, Emery SJ, Lewis MJ (2013) Influence of somatic state on cardiovascular measurements in pregnancy. Physiol Meas 35(1):15–29
- De Paco C, Ventura W, Oliva R, Miguel M, Arteaga A, Nieto A et al (2014) Umbilical artery Doppler at 19 to 22 weeks of gestation in the prediction of adverse pregnancy outcomes. Prenat Diagn 34(7):711–715
- Del Bene R, Barletta G, Mello G, Lazzeri C, Mecacci F, Parretti E et al (2001) Cardiovascular function in pregnancy: effects of posture. BJOG Int J Obstet Gynaecol. 108(4):344–52
- Dennis AT, Castro J, Carr C, Simmons S, Permezel M, Royse C (2012) Haemodynamics in women with untreated pre-eclampsia\*. Anaesthesia 67(10):1105–1118
- Desai DK, Moodley J, Naidoo DP (2004) Echocardiographic assessment of cardiovascular hemodynamics in normal pregnancy. Obstet Gynecol 104(1):20–29
- Deurloo KL, Bolte AC, Twisk JWR, van Vugt JMG (2009) Longitudinal Doppler measurements of spiral artery blood flow in relation to uterine artery blood flow. J Ultrasound Med Off J Am Inst Ultrasound Med 28(12):1623–1628
- Deutinger J, Rudelstorfer R, Bernaschek G (1988) Vaginosonographic velocimetry of both main uterine arteries by visual vessel recognition and pulsed Doppler method during pregnancy. Am J Obstet Gynecol 159(5):1072–1076



- Dickey RP (1995) Effect of ovulation induction on uterine blood flow and oestradiol and progesterone concentrations in early pregnancy. Human Reprod (Oxf, Engl) 10(11):2875–2879
- Dickey RP (1997) Doppler ultrasound investigation of uterine and ovarian blood flow in infertility and early pregnancy. Hum Reprod Update 3(5):467–503
- Dickey RP, Hower JF (1995) Ultrasonographic features of uterine blood flow during the first 16 weeks of pregnancy. Hum Reprod (Oxf, Engl) 10(9):2448–2452
- Dickey RP, Hower JF, Matulich EM, Brown GT (1994) Effect of standing on non-pregnant uterine blood flow. Ultrasound Obstet Gynecol Off J Int Soc Ultrasound Obstet Gynecol 4(6):480–487
- Dickey RP, Gasser RF, Hower JF, Matulich EM, Brown GT (1995) Relationship of uterine blood-flow to chorionic sac and embryo growth-rates. Hum Reprod (Oxf, Engl) 10(10):2676–2679
- Duvekot JJ, Cheriex EC, Pieters FAA, Peeters LLH (1995) Severely impaired fetal growth is preceded by maternal hemodynamic maladaptation in very early pregnancy. Acta Obstet Gynecol Scand 74(9):693–697
- Easterling TR, Benedetti TJ, Schmucker BC, Millard SP (1990) Maternal hemodynamics in normal and preeclamptic pregnancies: a longitudinal study. Obstet Gynecol 76(6):1061–1069
- Edgar JC. The practice of obstetrics: designed for the use of students and practitioners of medicine 1910
- Ergin RN, Yayla M (2015) Uterine artery pulsatility index and diastolic notch laterality according to the placental location. Clin Exp Obstet Gynecol 42(5):640–643
- Eser A, Zulfıkaroglu E, Eserdag S, Kılıc S, Danısman N (2011) Predictive value of middle cerebral artery to uterine artery pulsatility index ratio in preeclampsia. Arch Gynecol Obstet 284(2):307–311
- Estensen M-E, Grindheim G, Remme EW, Swillens A, Smiseth OA, Segers P et al (2012) Systemic arterial response and ventriculo-arterial interaction during normal pregnancy. Am J Hypertens 25(6):672–677
- Everett TR, Mahendru AA, McEniery CM, Wilkinson IB, Lees CC (2012) Raised uterine artery impedance is associated with increased maternal arterial stiffness in the late second trimester. Placenta 33(7):572–577
- Farina A, Rapacchia G, Freni Sterrantino A, Pula G, Morano D, Rizzo N (2011) Prospective evaluation of ultrasound and biochemical-based multivariable models for the prediction of late pre-eclampsia. Prenat Diagn 31(12):1147–1152
- Fernstrom I (1955) Arteriography of the uterine artery: its value in the diagnosis of uterine fibromyoma, tubal pregnancy, adnexal tumour, and placental site localization in cases of intra-uterine pregnancy. Acta Radiol Suppl 122:1–128
- Flo K, Wilsgaard T, Vårtun A, Acharya G (2010) A longitudinal study of the relationship between maternal cardiac output measured by impedance cardiography and uterine artery blood flow in the second half of pregnancy. BJOG Int J Obstet Gynaecol. 117(7):837–44
- Fugino Y, Ito F, Matuoka I, Kojima T, Koh B, Ogita S (1993)

  Pulsatility index of uterine artery in pregnant and nonpregnant women. Human Reproduction (oxford, England)
  8(7):1126-1128
- García B, Llurba E, Valle L, Gómez-Roig MD, Juan M, Pérez-Matos C et al (2016) Do knowledge of uterine artery resistance in the second trimester and targeted surveillance improve maternal and perinatal outcome? Ultrasound Obstet Gynecol Off J Int Soc Ultrasound Obstet Gynecol 47(6):680–689
- Geva T, Mauer MB, Striker L, Kirshon B, Pivarnik JM (1997) Effects of physiologic load of pregnancy on left ventricular contractility and remodeling. Am Heart J 133(1):53–59
- Gilson G, Samaan S, Crawford M, Quails C, Curet L (1997) Changes in hemodynamics, ventricular remodeling, and ventricular

- contractility during normal pregnancy: a longitudinal study. Obstet Gynecol 89(6):957–962
- Gleason RL, Taber LA, Humphrey JD (2004) A 2-D model of flowinduced alterations in the geometry, structure, and properties of carotid arteries. J Biomech Eng 126(3):371–381
- Gómez O, Martínez JM, Figueras F, Del Río M, Borobio V, Puerto B et al (2005) Uterine artery Doppler at 11–14 weeks of gestation to screen for hypertensive disorders and associated complications in an unselected population. Ultrasound Obstet Gynecol Off J Int Soc Ultrasound Obstet Gynecol 26(5):490–494
- Gómez O, Figueras F, Fernández S, Bennasar M, Martínez JM, Puerto B et al (2008) Reference ranges for uterine artery mean pulsatility index at 11–41 weeks of gestation. Ultrasound Obstet Gynecol Off J Int Soc Ultrasound Obstet Gynecol 32(2):128–132
- Guanes PP, Remohí J, Gallardo E, Valbuena D, Simón C, Pellicer A (1996) Age does not affect uterine resistance to vascular flow in patients undergoing oocyte donation. Fertil Steril 66(2):265–270
- Guedes-Martins L, Cunha A, Saraiva J, Gaio R, Macedo F, Almeida H (2014) Internal iliac and uterine arteries Doppler ultrasound in the assessment of normotensive and chronic hypertensive pregnant women. Sci Rep 4(1):3785–3788
- Hale SA, Schonberg A, Badger GJ, Bernstein IM (2009) Relationship between prepregnancy and early pregnancy uterine blood flow and resistance index. Reprod Sci (Thousand Oaks, Calif) 16(11):1091–1096
- Hennessy TG, MacDonald D, Hennessy MS, Maguire M, Blake S, McCann HA et al (1996) Serial changes in cardiac output during normal pregnancy: a Doppler ultrasound study. Eur J Obstet Gynecol Reprod Biol 70(2):117–122
- Jamal A, Abbasalizadeh F, Vafaei H, Marsoosi V, Eslamian L (2013) Multicenter screening for adverse pregnancy outcomes by uterine artery Doppler in the second and third trimester of pregnancy. Med Ultrason 15(2):95–100
- James JL, Chamley LW, Clark AR (2017) Feeding your baby in utero: How the uteroplacental circulation impacts pregnancy. Physiology (bethesda) 32(3):234–245
- Jauniaux E, Jurkovic D, Campbell S (1991) In vivo investigations of the anatomy and the physiology of early human placental circulations. Ultrasound Obstet Gynecol 1(6):435–445
- Jeffreys RM, Stepanchak W, Lopez B, Hardis J, Clapp JF (2006) Uterine blood flow during supine rest and exercise after 28 weeks of gestation. BJOG Int J Obstet Gynaecol. 113(11):1239–47
- Jones TB, Price RR, Gibbs SJ (1981) Volumetric determination of placental and uterine growth relationships from B-mode ultrasound by serial area-volume determinations. Invest Radiol 16(2):101–106
- Jurkovic D, Jauniaux E, Kurjak A, Hustin J, Campbell S, Nicolaides KH (1991) Transvaginal color Doppler assessment of the uteroplacental circulation in early pregnancy. Obstet Gynecol 77(3):365–369
- Kaihura C, Savvidou MD, Anderson JM, McEniery CM, Nicolaides KH (2009) Maternal arterial stiffness in pregnancies affected by preeclampsia. Am J Physiol: Heart Circ Physiol 297(2):H759–H764
- Kaminopetros P, Higueras MT, Nicolaides KH (1991) Doppler study of uterine artery blood flow: comparison of findings in the first and second trimesters of pregnancy. Fetal Diagn Ther 6(1–2):58–64
- Kamiya A, Togawa T (1980) Adaptive regulation of wall shear stress to flow change in the canine carotid artery. Am J Physiol: Heart Circ Physiol 239:H14-21
- Khalil A, Morales-Roselló J, Townsend R, Morlando M, Papageorghiou A, Bhide A et al (2016) Value of third-trimester cerebroplacental ratio and uterine artery Doppler indices as predictors of still-birth and perinatal loss. Ultrasound Obstet Gynecol Off J Int Soc Ultrasound Obstet Gynecol 47(1):74–80



- Kienast C, Moya W, Rodriguez O, Jijón A, Geipel A (2016) Predictive value of angiogenic factors, clinical risk factors and uterine artery Doppler for pre-eclampsia and fetal growth restriction in second and third trimester pregnancies in an Ecuadorian population. J Matern Fetal Neonatal Med 29(4):537–543
- Konje JC, Kaufmann P, Bell SC, Taylor DJ (2001) A longitudinal study of quantitative uterine blood flow with the use of color power angiography in appropriate for gestational age pregnancies. Am J Obstet Gynecol 185(3):608–613
- Kroon W, Huberts W, Bosboom M, van de Vosse F (2012) A numerical method of reduced complexity for simulating vascular hemodynamics using coupled 0D lumped and 1D wave propagation models. Comput Math Methods Med 2012(6):156094–156110
- Kuleva M, Youssef A, Maroni E, Contro E, Pilu G, Rizzo N et al (2011) Maternal cardiac function in normal twin pregnancy: a longitudinal study. Ultrasound Obstet Gynecol 38(5):575–580
- Kumar M, Gupta U, Bhattacharjee J, Singh R, Singh S, Goel M et al (2016) Early prediction of hypertension during pregnancy in a low-resource setting. Int J Gynaecol Obstet Off Organ Int Fed Gynaecol Obstet 132(2):159–164
- Lai J, Poon LCY, Pinas A, Bakalis S, Nicolaides KH (2013) Uterine Artery Doppler at 30–33 weeks' gestation in the prediction of preeclampsia. Fetal Diagn Ther 33(3):156–163
- Lakatta EG (2003) Arterial and cardiac aging: major shareholders in cardiovascular disease enterprises. Circulation 107(3):490–497
- Laurent S, Boutouyrie P, Cunha PG, Lacolley P, Nilsson PM (2019) Concept of extremes in vascular aging. Hypertension 74(2):218–228
- Leite JF, Lobo GAR, Nowak PM, Antunes IR, Araujo Júnior E (2019) Pares DBS Prediction of preeclampsia in the first trimester of pregnancy using maternal characteristics, mean arterial pressure, and uterine artery Doppler data in a Brazilian population. Obstet Gynecol Sci. 62(6):391–396
- Lof M, Olausson H, Bostrom K, Janerot-Sjöberg B, Sohlstrom A, Forsum E (2005) Changes in basal metabolic rate during pregnancy in relation to changes in body weight and composition, cardiac output, insulin-like growth factor I, and thyroid hormones and in relation to fetal growth. Am J Clin Nutr 81(3):678–685
- Mabie WC, DiSessa TG, Crocker LG, Sibai BM, Arheart KL (1994) A longitudinal study of cardiac output in normal human pregnancy. Am J Obstet Gynecol 170(3):849–856
- Mahendru AA, Everett TR, Wilkinson IB, Lees CC, McEniery CM (2014) A longitudinal study of maternal cardiovascular function from preconception to the postpartum period. J Hypertens 32(4):849–856
- Mahendru AA, Foo FL, McEniery CM, Everett TR, Wilkinson IB, Lees CC (2017) Change in maternal cardiac output from preconception to mid-pregnancy is associated with birth weight in healthy pregnancies. Ultrasound Obstet Gynecol 49(1):78–84
- Mäkikallio K, Tekay A, Jouppila P (2004) Uteroplacental hemodynamics during early human pregnancy: a longitudinal study. Gynecol Obstet Invest 58(1):49–54
- Meah VL, Cockcroft JR, Backx K, Shave R, Stöhr EJ (2016) Cardiac output and related haemodynamics during pregnancy: a series of meta-analyses. Heart 102(7):518
- Mesa A, Jessurun C, Hernandez A, Adam K, Brown D, Vaughn WK et al (1999) Left ventricular diastolic function in normal human pregnancy. Circulation 99(4):511–517
- Mo LYL, Bascom PAJ, Ritchie K, McCowan LME (1988) A Transmission-Line Modeling Approach to the Interpretation of Uterine Doppler Waveforms. Ultrasound Med Biol 14(5):365–376
- Moertl MG, Schlembach D, Papousek I, Hinghofer-Szalkay H, Weiss EM, Lang U et al (2012) Hemodynamic evaluation in pregnancy: limitations of impedance cardiography. Physiol Meas 33(6):1015–1026

- Mone SM, Sanders SP, Colan SD (1996) Control Mechanisms for physiological hypertrophy of pregnancy. Circulation 94(4):667–672
- Nevo O, Soustiel JF, Thaler I (2010) Maternal cerebral blood flow during normal pregnancy: a cross-sectional study. Am J Obstet Gynecol 203(5):475.e1-475.e6
- Nii M, Ishida M, Dohi K, Tanaka H, Kondo E, Ito M et al (2018) Myocardial tissue characterization and strain analysis in healthy pregnant women using cardiovascular magnetic resonance native T1 mapping and feature tracking technique. J Cardiov Magn Reson 20(1):52
- Novelli GP, Vasapollo B, Gagliardi G, Tiralongo GM, Pisani I, Manfellotto D et al (2012) Left ventricular midwall mechanics at 24 weeks' gestation in high-risk normotensive pregnant women: relationship to placenta-related complications of pregnancy. Ultrasound Obstet Gynecol 39(4):430–437
- Odibo AO, Zhong Y, Goetzinger KR, Odibo L, Bick JL, Bower CR et al (2011) First-trimester placental protein 13, PAPP-A, uterine artery Doppler and maternal characteristics in the prediction of pre-eclampsia. Placenta 32(8):598–602
- Ogueh O, Brookes C, Johnson MR (2009) A Longitudinal study of the maternal cardiovascular adaptation to spontaneous and assisted conception pregnancies. Hypertens Pregnancy 28(3):273–289
- Oliveira N, Magder LS, Blitzer MG, Baschat AA (2014) First-trimester prediction of pre-eclampsia: external validity of algorithms in a prospectively enrolled cohort. Ultrasound Obstet Gynecol Off J Int Soc Ultrasound Obstet Gynecol 44(3):279–285
- Olofsson P, Laurini RN, Marsál K (1993) A high uterine artery pulsatility index reflects a defective development of placental bed spiral arteries in pregnancies complicated by hypertension and fetal growth retardation. Eur J Obstet Gynecol Reprod Biol 49(3):161–168
- Osol G, Mandala M (2009) Maternal uterine vascular remodeling during pregnancy. Physiology (bethesda) 24(1):58–71
- Osol G, Moore LG (2014) Maternal uterine vascular remodeling during pregnancy. Microcirculation (New York, NY: 1994) 21(1):38–47
- Oyama-Kato M, Ohmichi M, Takahashi K, Suzuki S, Henmi N, Yokoyama Y et al (2006) Change in pulse wave velocity throughout normal pregnancy and its value in predicting pregnancy-induced hypertension: a longitudinal study. Am J Obstet Gynecol 195(2):464–469
- Özkaya Ü, Özkan S, Özeren S, Çorakçı A (2007) Doppler examination of uteroplacental circulation in early pregnancy: Can it predict adverse outcome? J Clin Ultrasound 35(7):382–386
- Palmer SK, Zamudio S, Coffin C, Parker S, Stamm E, Moore LG (1992) Quantitative estimation of human uterine artery blood flow and pelvic blood flow redistribution in pregnancy. Obstet Gynecol 80(6):1000–1006
- Perry H, Lehmann H, Mantovani E, Thilaganathan B, Khalil A (2020) Are maternal hemodynamic indices markers of fetal growth restriction in pregnancies with a small-for-gestational-age fetus? Ultrasound Obstet Gynecol 55(2):210–216
- Pilalis A, Souka AP, Antsaklis P, Daskalakis G, Papantoniou N, Mesogitis S et al (2007) Screening for pre-eclampsia and fetal growth restriction by uterine artery Doppler and PAPP-A at 11–14 weeks' gestation. Ultrasound Obstet Gynecol Off J Int Soc Ultrasound Obstet Gynecol 29(2):135–140
- Plasencia W, González-Dávila E, Lorenzo AG, Armas-González M, Padrón E, González-González NL (2015) First trimester placental volume and vascular indices in pregnancies complicated by preeclampsia. Prenat Diagn 35(12):1247–1254
- Ponmozhi G, Keepanasseril A, Mathaiyan J, Manikandan K (2019) Nitric oxide in the prevention of pre-eclampsia (NOPE): A double-blind randomized placebo-controlled trial assessing the efficacy of isosorbide mononitrate in the prevention of



- pre-eclampsia in high-risk women. J Obstet Gynaecol India 69(Suppl 2):103-110
- Poon LCY, Kametas NA, Maiz N, Akolekar R, Nicolaides KH (2009a) First-trimester prediction of hypertensive disorders in pregnancy. Hypertension 53(5):812–818
- Poon LCY, Karagiannis G, Leal A, Romero XC, Nicolaides KH (2009b) Hypertensive disorders in pregnancy: screening by uterine artery Doppler imaging and blood pressure at 11–13 weeks. Ultrasound Obstet Gynecol Off J Int Soc Ultrasound Obstet Gynecol 34(5):497–502
- Poppas A, Shroff SG, Korcarz CE, Hibbard JU, Berger DS, Lindheimer MD et al (1997) Serial assessment of the cardiovascular system in normal pregnancy: role of arterial compliance and pulsatile arterial load. Circulation 95(10):2407–2415
- Prajapati SR, Maitra N (2013) Prediction of pre-eclampsia by a combination of maternal history, uterine artery Doppler, and mean arterial pressure (a prospective study of 200 cases). J Obstet Gynaecol India 63(1):32–36
- Prodan N, Wagner P, Sonek J, Hoopmann M, Mutz A, Brucker S et al (2019) First trimester uterine artery pulsatility index levels in euploid and aneuploid pregnancies. Arch Gynecol Obstet 300(6):1559–1564
- Rang S, Lapiedra BP, Montfrans GA, Bouma BJ, Wesseling KH, Wolf H (2007) Modelflow: a new method for noninvasive assessment of cardiac output in pregnant women. Am J Obstet Gynecol. 196(3):235.e1-235.e8
- Rang S, Montfrans GA, Wolf H (2008) Serial hemodynamic measurement in normal pregnancy, preeclampsia, and intrauterine growth restriction. Am J Obstet Gynecol. 198(5):519.e1-519.e9
- Reymond P, Merenda F, Perren F, Rüfenacht D, Stergiopulos N (2009) Validation of a one-dimensional model of the systemic arterial tree. Am J Physiol: Heart Circ Physiol 297(1):H208–H222
- Rigano S, Ferrazzi E, Boito S, Pennati G, Padoan A, Galan H (2010) Blood flow volume of uterine arteries in human pregnancies determined using 3D and bi-dimensional imaging, angio-Doppler, and fluid-dynamic modeling. Placenta 31(1):37–43
- Robb AO, Mills NL, Din JN, Smith IBJ, Paterson F, Newby DE et al (2009) Influence of the menstrual cycle, pregnancy, and preeclampsia on arterial stiffness. Hypertension 53(6):952–958
- Robertson WB (1976) Uteroplacental vasculature. J Clin Pathol Suppl (r Coll Pathol) 10:9–17
- Robson SC, Hunter S, Boys RJ, Dunlop W (1989) Serial study of factors influencing changes in cardiac output during human pregnancy. Am J Physiol 256(4 Pt 2):H1060–H1065
- Sagol S, Özkinay E, Öztekin K, Özdemir N (1999) The Comparison of uterine artery Doppler velocimetry with the Histopathology of the Placental Bed. Aust N Z J Obstet Gynaecol 39(3):324–329
- Savu O, Jurcuţ R, Giuşcă S, van Mieghem T, Gussi I, Popescu BA et al (2012) Morphological and functional adaptation of the maternal heart during pregnancy. Circ Cardiovasc Imaging 5(3):289–297
- Savvidou MD, Kaihura C, Anderson JM, Nicolaides KH (2011) Maternal arterial stiffness in women who subsequently develop preeclampsia. PloS ONE 6(5):e18703
- Scazzocchio E, Figueras F, Crispi F, Meler E, Masoller N, Mula R et al (2013) Performance of a first-trimester screening of preeclampsia in a routine care low-risk setting. Am J Obstet Gynecol. 208(3):203.e1-203.e10
- Schannwell CM, Zimmermann T, Schneppenheim M, Plehn G, Marx R, Strauer BE (2002) Left ventricular hypertrophy and diastolic dysfunction in healthy pregnant women. Cardiology 97(2):73–78
- Sciscione AC, Hayes EJ, Medicine SM-F (2009) Uterine artery Doppler flow studies in obstetric practice. Am J Obstet Gynecol 201(2):121-6
- Sengupta SP, Bansal M, Hofstra L, Sengupta PP, Narula J (2017) Gestational changes in left ventricular myocardial contractile

- function: new insights from two-dimensional speckle tracking echocardiography. Int J Cardiovasc Imaging 33(1):69-82
- Simmons LA, Gillin AG, Jeremy RW (2002) Structural and functional changes in left ventricle during normotensive and preeclamptic pregnancy. Am J Physiol Heart C 283(4):H1627–H1633
- Stergiopulos N, Young DF, Rogge TR (1992) Computer simulation of arterial flow with applications to arterial and aortic stenoses. J Biomech 25(12):1477–1488
- Tekay A, Martikainen H, Jouppila P (1996) Comparison of uterine blood flow characteristics between spontaneous and stimulated cycles before embryo transfer. Hum Reprod (Oxf, Engl) 11(2):364–368
- Tezcan ME, Temizkan O, Ozderya A, Melikoglu M, Aydin K, Sargin M et al (2015) Color Doppler analysis of female reproductive vasculature in Behçet's disease. Reumatismo 67(3):103–108
- Thaler I, Manor D, Itskovitz J, Rottem S, Levit N, Timor-Tritsch I et al (1990) Changes in uterine blood flow during human pregnancy. Am J Obstet Gynecol 162(1):121–125
- Valensise H, Novelli GP, Vasapollo B, Borzi M, Arduini D, Galante A et al (2000) Maternal cardiac systolic and diastolic function: relationship with uteroplacental resistances. A Doppler and echocardiographic longitudinal study. Ultrasound Obstet Gynecol 15(6):487–97
- Valensise H, Novelli GP, Vasapollo B, Ruzza GD, Romanini ME, Marchei M et al (2001) Maternal diastolic dysfunction and left ventricular geometry in gestational hypertension. Hypertension 37(5):1209–1215
- Valensise H, Vasapollo B, Novelli GP, Pasqualetti P, Galante A, Arduini D (2006) Maternal total vascular resistance and concentric geometry: a key to identify uncomplicated gestational hypertension. BJOG Int J Obstet Gynaecol. 113(9):1044–52
- Valensise H, Vasapollo B, Gagliardi G, Novelli GP (2008) Early and late preeclampsia. Hypertension 52(5):873–880
- Valentin L, Sladkevicius P, Laurini R, Söderberg H, Marsál K (1996) Uteroplacental and luteal circulation in normal first-trimester pregnancies: Doppler ultrasonographic and morphologic study. Am J Obstet Gynecol 174(2):768–775
- van den Boom T, Stevens R, Delhaas T, van de Vosse F, Huberts W (2018) Zero-dimensional lumped approach to incorporate the dynamic part of the pressure at vessel junctions in a 1D wave propagation model. Int J Numer Methods Biomed Eng 34(9):e3116
- van der Graaf A, Cuffie-Jackson C, Vissers MN, Trip MD, Gagné C, Shi G et al (2008) Efficacy and safety of coadministration of Ezetimibe and simvastatin in adolescents with heterozygous familial hypercholesterolemia. J Am Coll Cardiol 52(17):1421–1429
- Vårtun Å, Flo K, Acharya G (2014) Effect of passive leg raising on systemic hemodynamics of pregnant women: a dynamic assessment of maternal cardiovascular function at 22–24 weeks of gestation. PLoS ONE. 9(4):e94629
- Vasapollo B, Novelli GP, Valensise H (2008) Total vascular resistance and left ventricular morphology as screening tools for complications in pregnancy. Hypertension 51(4):1020–1026
- Vinayagam D, Thilaganathan B, Stirrup O, Mantovani E, Khalil A (2018) Maternal hemodynamics in normal pregnancy: reference ranges and role of maternal characteristics. Ultrasound Obstet Gynecol 51(5):665–671
- Vlahović-Stipac A, Stankić V, Popović ZB, Putniković B, Nešković AN (2010) Left ventricular function in gestational hypertension: serial echocardiographic study. Am J Hypertens 23(1):85–91
- Wan W, Gleason RL (2013) Dysfunction in elastic fiber formation in fibulin-5 null mice abrogates the evolution in mechanical response of carotid arteries during maturation. Am J Physiol Heart Circ Physiol 304(5):H674–H686



- Wang L, Qiao J, Li R, Zhen X, Liu Z (2010) Role of endometrial blood flow assessment with color Doppler energy in predicting pregnancy outcome of IVF-ET cycles. Reprod Biol Endocrinol 8(1):122–127
- Willeit P, Tschiderer L, Allara E, Reuber K, Seekircher L, Gao L et al (2020) Carotid intima-media thickness progression as surrogate marker for cardiovascular risk: meta-analysis of 119 clinical trials involving 100 667 patients. Circulation 142(7):621–642
- Wilson MJ, Lopez M, Vargas M, Julian C, Tellez W, Rodriguez A et al (2007) Greater uterine artery blood flow during pregnancy in multigenerational (Andean) than shorter-term (European) high-altitude residents. Am J Physiol Regul Integr Comp Physiol 293(3):R1313–R1324
- Woessner JF, Brewer TH (1963) Formation and breakdown of collagen and elastin in the human uterus during pregnancy and post-partum involution. Biochem J 89(1):75–82
- Wolfe LA, Preston RJ, Burggraf GW, McGrath MJ (1999) Effects of pregnancy and chronic exercise on maternal cardiac structure and function. Can J Physiol Pharmacol 77(11):909–917
- Yalti S, Gürbüz B, Ficicioglu C, Canova H (2003) Doppler evaluation of the uterine, intraovarian, stromal and spiral arteries on the day of human chorionic gonadotrophin administration in controlled

- ovarian hyperstimulation. J Obstet Gynaecol J Inst Obst Gynaecol 23(4):402-406
- Yu CKH, Khouri O, Onwudiwe N, Spiliopoulos Y, Nicolaides KH, Group FMFS-TS (2008) Prediction of pre-eclampsia by uterine artery Doppler imaging: relationship to gestational age at delivery and small-for-gestational age. Ultrasound Obstet Gynecol Off J Int Soc Ultrasound Obstet Gynecol 31(3):310–3
- Zamudio S, Palmer SK, Droma T, Stamm E, Coffin C, Moore LG (1995) Effect of altitude on uterine artery blood flow during normal pregnancy. J Appl Physiol (Bethesda, MD: 1985) 79(1):7–14
- Zebitay AG, Tutumlu M, Verit FF, Ilhan GK, Gungor ES, Cetin O et al (2016) A comparative analysis of arterial blood flow in unexplained infertility, tubal infertility and fertile groups. Gynecol Endocrinol Off J Int Soc Gynecol Endocrinol 32(6):442–445
- Zieman SJ, Melenovsky V, Kass DA (2005) Mechanisms, pathophysiology, and therapy of arterial stiffness. Arterioscler Thromb Vasc Biol 25(5):932–943

**Publisher's Note** Springer Nature remains neutral with regard to jurisdictional claims in published maps and institutional affiliations.

